Title page

Manuscript title

Prdm1 Positively Regulates Liver Group 1 ILCs Cancer Immune Surveillance and Preserves Functional Heterogeneity

Authors and affiliations

Jitian He[1], Le Gao[1], Peiying Wang[1], Wing Keung Chan[4], Yiran Zheng[1], Yumo Zhang[1], Jiming Wang[5], Huaiyong Chen[3,6,7], Zhouxin Yang[2], Youwei Wang[1]

[1]Institute of Medical Engineering & Translational Medicine, Tianjin University, Tianjin 300072, China.

[2]Zhejiang Provincial Key Lab of Geriatrics and Geriatrics Institute of Zhejiang Province, Zhejiang Hospital, Hangzhou 310030, China.

[3]College of Pulmonary and Critical Care Medicine, 8th Medical Center, Chinese PLA General Hospital, Beijing, China

[4]Department of Internal Medicine, Division of Hematology, The Ohio State University, Columbus, OH 43210, USA.

[5]Tianjin Economic-Technological Development Area (TEDA) Hospital, Tianjin 300451, China

[6]Department of Basic Medicine, Haihe Hospital, Tianjin University, Tianjin 300350, China.

[7]Tianjin Key Laboratory of Lung Regenerative Medicine, Tianjin 300350, China.

Authorship notes: JH, LG, and PW contributed equally to this work.

Co-corresponding authors: Huaiyong Chen (huaiyong.chen@foxmail.com), Zhouxin Yang (yangzhouxin@hotmail.com), Youwei Wang (youwei.wang@tju.edu.cn)

Address correspondence to: Youwei Wang, Institute of Medical Engineering & Translational Medicine, Tianjin University, Tianjin 300072, China. Email: youwei.wang@tju.edu.cn. Or to Zhouxin Yang, Zhejiang Provincial Key Lab of Geriatrics and Geriatrics Institute of Zhejiang Province, Zhejiang Hospital, Hangzhou 310030, China. Email: yangzhouxin@hotmail.com. Or to Huaiyong Chen, Department of Basic Medicine, Haihe Hospital, Tianjin University, Tianjin 300350, China. Email: huaiyong.chen@foxmail.com.

Abstract

Group 1 innate lymphoid cells (ILCs) comprise conventional natural killer (cNK) cells and type 1 innate lymphoid cells (ILC1s). The main functions of liver cNK cells and ILC1s not only include directly killing target cells but also regulating local immune microenvironment of the liver through the secretion of cytokines. Uncovering the intricate mechanisms by which transcriptional factors regulate and influence the functions of liver cNK cells and ILC1s, particularly within the context of liver tumors, presents a significant opportunity to amplify the effectiveness of immunotherapies against liver malignancies. Using Ncr1-drived conditional knockout mouse model, our study reveals the regulatory role of *Prdm1* in shaping the composition and maturation of cNK cells. Although *Prdm1* did not affect the killing function of cNK cells in an *in vivo* cytotoxicity model, a significant increase in cancer metastasis was observed in *Prdm1* knockout mice. Interferon-gamma (IFN-γ), granzyme B, and perforin secretion decreased significantly in *Prdm1* deficient cNK cells and liver ILC1s. scRNA sequencing data also provided evidences that Prdm1 maintains functional subsets of cNK cells and liver ILC1s and facilitates communications between cNK cells, liver ILC1s and macrophages. The present study unveiled a novel regulatory mechanism of Prdm1 in cNK cells and liver ILC1s, showing promising potential for developing innovative immune therapy strategies against liver cancer.

Main text

Introduction

Group 1 ILCs consist of cNK cells and ILC1s (1, 2), with distinct developmental trajectories and effect molecules (3). Both cNK cells and ILC1s play indispensable roles in combatting viral infections (4), maintaining local immune homeostasis (5), eradicating malignant transformed cells (6), and fostering cross-talk with adaptive immunity (7). cNK cells demonstrate potent cellular cytotoxicity, facilitating direct elimination of target cells (8). On the contrary, a defining attribute of ILC1s is their predominant cytokine-mediated functions, with limited cellular killing capacity (9). In a state of homeostasis, liver group 1 ILCs ($CD45^{+}CD3^{-}NK1.1^{+}NKp46^{+}$) can be discriminated into cNK cells and ILC1s by the differential expression of CD49a and CD49b (2): cNK cells are marked by the expression of CD49b, while liver ILC1s exhibit a distinctive positivity for CD49a. Tumor Necrosis Factor Related Apoptosis Inducing Ligand (TRAIL) is also expressed on liver ILC1s, but not on cNK cells (10). Transcriptional factors (TFs) such as T-bet, Nfil3, PLZF, and ID2 are required for cNK cells and liver ILC1s development or generation of their progenitors (11-14). Eomes is considered to be necessary for NK cell maturation, but not for ILC1s (15). Liver environment facilitated T-bet expression in the early stage of NK cells development, which results in Eomes repression. The repression of T-bet is required for $Eomes^{+}$ NK cells (16). On the contrary, deficiency of Hobit results in the depletion of ILC1s, while only leaving little impact on liver NK cells (17). These studies suggest that some TFs may, or usually, play different roles in NK cells and ILC1s.

During the development of liver cancers, the functions of immune cells are often inhibited,

resulting in the formation of an immunosuppressive tumor microenvironment, and sometimes even systemic immune suppression (18). Transforming a cold tumor into a hot tumor with a stronger immune response is one of the goals of many cancer immunotherapies (19). Research targeting the immune system is showing increasing clinical promise in liver cancer treatment (20). One of our recent studies also found that Toll-like receptor agonists can significantly enhance the anti-tumor effect of Sorafenib by reconstructing the tumor immune microenvironment and reshaping the vascular system (21).

The anti-tumor activity of cNK cells in the liver is relatively well-established, whereas the relationship between liver ILC1 and tumors is still a topic of controversy. Clinical data showed that liver tumors with a higher infiltration of NK cells are associated with a better prognosis (22). Decreased NK cell activity is closely correlated with the malignancy of liver tumors and represents a significant risk factor for recurrence (23). The tumor microenvironment orchestrates the transformation of cNK cells into ILC1s in a TGF-β-dependent manner, resulting in their diminished capacity to control tumor growth and metastasis. This process ultimately promotes tumor immunoevasion (24). However, researches also revealed that, distinct from directly inhibiting tumor growth, the primary function of ILC1 is to suppress the seeding of metastatic tumor cells in liver tissue (6). Comprehensive research in this field is essential to harness the precision of group 1 ILCs targeted immunotherapy for liver cancers.

The transcription factor network governs the function of group 1 ILCs and the balance between cNK and ILC1. Our research team, along with others, has observed that one of the transcription factor in TGF-β pathway, Smad4, promotes the shift in balance from cNK cells towards ILC1 in a TGF-beta-independent pathway, and simultaneously, it positively regulates the expression of

another transcription factor, PR domain 1 (Prdm1/Blimp1) (25, 26). Prdm1 plays a crucial role in the differentiation of B cells into plasma cells and the homeostasis of T cells (27-29). The function and regulatory network of Prdm1 in NK cells is distinct from B cells and T cells, for its expression is independent of B-cell lymphoma 6 (Bcl-6) and Interferon Regulatory actor 4 (IRF4) but relies on T-bet. In the study that identified Prdm1 as an essential transcriptional factor for NK cell maturation (30), no significant differences were observed in IFN-γ production or cytotoxicity between Prdm1-deficient and wild-type NK cells. Although Prdm1 expression is dependent on IL-15 in immature NK cells and can be further upregulated by IL-12 or IL-21, it plays a role in downregulating the expression of certain cytokine receptors, such as CD25, consequently diminishing the responsiveness of NK cells to IL-2 (31). Notably, some studies even suggested that Prdm1 suppressed the secretion of IFN-γ in NK cells (32). These findings imply that, although Prdm1 promotes NK cell development, it may function as a negative regulator of their activity. However, direct evidence supporting the impact of Prdm1 on NK cell anti-tumor capabilities is still lacking. Furthermore, there has been no investigation into its influence on the homeostasis of cNK cells and ILC1s in the liver, nor has there been an exploration of the underlying mechanisms.

In the current study, we found that the deletion of *Prdm1* in Ncr1^{+} cells resulted in an imbalance in the homeostasis of liver group 1 ILCs, with a shift towards cNK cells. The data also support the essential role of Prdm1 in the cancer surveillance mediated by cNK cells. While Prdm1 positively regulates genes associated with cellular cytotoxicity, it concurrently exerts inhibitory control over certain positive regulators of NK cell development and functionality, such as JunB. Using single-cell RNA sequencing, we have identified a subset of cNK cells within the liver characterized by elevated JunB expression. These cells exhibit decreased expression of genes associated with cellular

115 cytotoxicity, and their abundance significantly increases following Prdm1 knockout. Furthermore,
116 our data also support that Prdm1 promotes the cross-talk between group 1 ILCs and macrophages.

117 **Results**

118 ***Prdm1* promotes group 1 ILCs homeostasis and terminal maturation**

119 Examination of 363 liver hepatocellular carcinoma (LIHC) patient samples from The Cancer
120 Genome Atlas (TCGA) revealed a positive correlation between the expression of NK cell-associated
121 genes (33) (*NCR1*, *KLRB1*, *CD160*, *PRF1,* etc.) and *PRDM1* expression (Figure 1A). The patients
122 are ordered from highest to lowest based on the expression of NK-Prdm1 for survival analysis
123 (Figure 1B). Notably, patients exhibiting higher levels of NK-PRDM1 expression (above the median)
124 experienced better survival outcomes compared to those with lower levels of NK-PRDM1
125 expression (below the median) (Figure 1C). Similar results were also found in skin cutaneous
126 melanoma (SKCM, n=454) and lung adenocarcinoma (LUAD, n=497) patients (Supplemental
127 Figure 1, A-F). Patients within the highest quartile of NK-PRDM1 signature expression
128 demonstrated enhanced overall survival, a result that achieved statistical significance in LUAD and
129 SKCM patients (Supplemental Figure 1, G-I). These data suggested that *PRDM1* in NK cells might
130 be essential for immune surveillance in solid tumors, including liver cancer, and prompted us to
131 investigate the function and mechanism of *PRDM1* in NK cells and ILC1 within the context of liver
132 cancer.

133 *Ncr1-Cre* mice were crossed with $Prdm1^{fl/fl}$ mice to generate *Ncr1-cre* $Prdm1^{fl/fl}$ mice, which
134 specifically knockout exons 6-8 of *Prdm1* (34) in NKp46 positive cells (Figure 1D). The mice
135 carrying $Ncr1^{Cre/+}Prdm1^{fl/fl}$ were referred to as $Prdm1^{\Delta Ncr1}$ mice, and the mice carrying

136 *Ncr1*$^{+/+}$*Prdm1*$^{fl/fl}$ were referred to as *Prdm1*$^{+/+}$ mice or wild-type (WT) mice. To further validate the

137 deletion of *Prdm1* in NKp46^{+} cells of *Prdm1*$^{\Delta Ncr1}$ mice, CD3^{-}NK1.1^{+}NKp46^{+} cells were sorted and

138 the expression of *Prdm1* was measured by real-time RT-PCR. The expression of *Prdm1* was almost

139 undetectable in CD3^{-}NK1.1^{+}NKp46^{+} cells of *Prdm1*$^{\Delta Ncr1}$ mice, while was similar between total

140 splenocytes in *Prdm1*$^{+/+}$ and *Prdm1*$^{\Delta Ncr1}$mice (Figure 1, E and F) indicating successful, and

141 specifical knockout of *Prdm1* in NKp46^{+} cells.

142 Proportion and absolute number of cNK cells in blood, bone marrow, lung, liver, spleen, and

143 lymph nodes were analyzed by flow cytometry. Compared with *Prdm1*$^{+/+}$ mice, the percentage and

144 absolute number of cNK cells (CD45^{+}CD3^{-}NK1.1^{+}NKp46^{+}) among lymphocytes was decreased in

145 all of these tissues, whereas increased number of NK cells were observed in bone marrow (Figure

146 1G; Supplemental Figure 2A). NK cell terminal maturation can be divided into four stages according

147 to the expression of CD11b and CD27 (35). Stage IV (CD11b^{+}CD27^{-}) NK cells show higher level

148 of effector molecules than any other stages and are considered as the most mature NK cells (36).

149 The maturation of cNK cells (gated by CD45^{+}CD3^{-}NK1.1^{+}NKp46^{+}CD49b^{+}) from blood, bone

150 marrow, lung, liver, spleen, and lymph nodes were assessed, based on the expression of CD11b and

151 CD27. Compared with *Prdm1*$^{+/+}$ mice, the proportion of the most mature CD11b^{+}CD27^{-} NK cells

152 were significantly decreased in all of the analyzed tissues in *Prdm1*$^{\Delta Ncr1}$ mice (Figure 1H;

153 Supplemental Figure 2B). Killer cell lectin-like receptor subfamily G member 1 (KLRG1) is a

154 lectin-like receptor which was considered as another marker of NK cell maturation (37). In both

155 *Prdm1*$^{+/+}$ and *Prdm1*$^{\Delta Ncr1}$ mice, cNK cells from the liver and lung had the highest expression of

156 KLRG1, following by blood and spleen (Supplemental Figure 2C). The lowest KLRG1 expression

157 was observed in cNK cells derived from lymph nodes and bone marrow, indicating the presence of

158 the most immature cNK cells in these tissues. Consistent with CD11b/CD27 based maturation
159 analysis, a significant loss of KLRG1^{+} NK cells in cNK cells was observed in *Prdm1*$^{\Delta Ncr1}$ mice
160 (Supplemental Figure 2C). Together, these data comfired that *Prdm1* is required for the terminal
161 maturation of cNK cells among various tissues.

162 ***Prdm1* is required for group 1 ILCs to control tumor metastasis**

163 Two subpopulations of liver group 1 ILCs (gated by CD45^{+}CD3^{-}NK1.1^{+}NKp46^{+}) were further
164 analyzed based on the expression of CD49a and CD49b (Figure 2A). Compared with *Prdm1*$^{+/+}$ mice,
165 the *Prdm1*$^{\Delta Ncr1}$ mice exhibited an increased percentage of cNK cells (CD49a^{-}CD49b^{+}) and reduced
166 proportion of ILC1s (CD49a^{+}CD49b^{-}) (Figure 2A). Of note, the absolute number of both cNK cells
167 and ILC1s were decreased in *Prdm1*$^{\Delta Ncr1}$ mice, with a more robustly reduction in ILC1s (Figure 2A),
168 which underscored the crucial role of *Prdm1* in maintaining the quantity of both liver cNK cells and
169 ILC1s. Expression level of CD49b was slightly upregulated in *Prdm1*$^{\Delta Ncr1}$ cNK cells and NKp46^{+}
170 cells in the liver and other tissues (Supplemental Figure 2, D and E). Increased CD49a expression
171 was also observed in *Prdm1*$^{\Delta Ncr1}$ liver ILC1s, while it showed decreased expression in NKp46^{+} cells
172 in the liver, bone marrow, and lymph nodes (Supplemental Figure 2, F and G). These results
173 indicated the essential role of Prdm1 in maintaining the balance and hemostasis of cNK cells and
174 ILC1s.

175 The decreased quantity of NK cell homeostasis and maturation of cNK cells due to *Prdm1* loss
176 motivated us to further explore whether deficiency of Prdm1 impaired NK cell cytotoxicity. A B2M-
177 deficient cell-based *in vivo* cytotoxicity assay was used to evaluate the effect of *Prdm1* on the
178 cytotoxicity of NK cells (38, 39). B2M-deficient cells do not have detectable Major

179 Histocompatibility Complex I (MHC-I) on the cell surface, making them the target of NK cells (40).
180 Health NK cells will reject B2M-deficient donor cells efficiently and the elimination was used to
181 quantify the cytotoxicity of NK cells. Although significant impaired homeostasis and maturation of
182 NK cells were observed in *Prdm1*$^{\Delta Ncr1}$ mice, no significant difference in the *in vivo* cytotoxicity
183 assay were observed between *Prdm1*$^{+/+}$ and *Prdm1*$^{\Delta Ncr1}$ mice (Supplemental Figure 2, H and I).
184 Besides their direct cytotoxic capabilities, NK cells' anti-tumor potential is also influenced by
185 additional factors. These include their ability to counteract tumor-induced immune suppression and
186 exhaustion, enhancing their effectiveness against cancer cells. Furthermore, NK cells can secrete
187 cytokines that activate other immune cells, thereby orchestrating a broader immune response for the
188 elimination of tumors. Moreover, the cytotoxicity assay, due to its relatively short duration, might
189 not fully represent the anti-tumor activity of NK cells when continuously exposed to immune
190 inhibitory signals in the tumor microenvironment. Therefore, we initiated an *in vivo* tumor model
191 to further investigate the impact of *Prdm1* on NK cell anti-tumor capability. B16F10 is a melanoma
192 cell line with low expression of MHC-I, which was susceptible to NK cell killing and usually used
193 to evaluate NK cell anti-tumor capacity (41-43). The B16F10 cells were intravenously (for lung
194 metastasis) or intrasplenic (for liver metastasis) administrated in the mice. The melanoma nodes
195 were quantified three (intravenous injection) or two (intrasplenic injection) weeks after tumor
196 inoculation. Compared with *Prdm1*$^{+/+}$ mice, deficiency of *Prdm1* resulted in more metastasis
197 nodules in both lung (~ 2-fold) and liver (~ 4-fold) (Figure 2, B and D). Histological analysis further
198 confirmed the increased frequency of metastasis tumor foci in *Prdm1*$^{\Delta Ncr1}$ mice (Figure 2, C and E).
199 In agreement with our *in vivo* data, we also observed decreased IFN-γ secretion in *Prdm1*$^{\Delta Ncr1}$ mice-
200 derived splenic cNK cells, liver cNK cells, and liver ILC1s when stimulated by IL-18 alone or IL-

201 12/IL-18 (Figure 2F; Supplemental Figure3; Supplemental Figure 12B), which indicated that *Prdm1*
202 is required for full activation of cNK cells and ILC1s in the context of IFN-γ production. These data
203 implying that *Prdm1* is indispensable for NK cell mediated tumor surveillance.

204 **Bulk RNA-seq depicts *Prdm1*-mediated functions in cNK cells**

205 Bulk RNA sequencing of splenic cNK cells ($CD3^{-}NK1.1^{+}NKp46^{+}$) was conducted to uncover
206 the molecular mechanisms by which *Prdm1* regulates NK cell anti-tumor immunity (Figure 3A).
207 Differentially expressed genes (DEGs) between $Prdm1^{+/+}$ and $Prdm1^{\Delta Ncr1}$ mice were determined
208 using a criterion of $\log_2$ (fold change) > 0.5 and $P < 0.05$. 445 DEGs were identified out of 17434
209 protein-coding genes, which consisted of 223 upregulated genes and 222 downregulated genes
210 (Figure 3B).

211 Gene Ontology (GO) analysis revealed the enrichment of glucuronate metabolism and
212 lymphocyte differentiation in upregulated genes in $Prdm1^{\Delta Ncr1}$ mice derived NK cells (Figure 3C),
213 both of which were associated with cellular growth and development. In contrast, leukocyte mediate
214 cytotoxicity, immune receptor activity, and integrin binding was enriched in the genes which
215 decreased their expression level in in $Prdm1^{\Delta Ncr1}$ mice (Figure 3C).

216 Gene Set Enrichment Analysis (GSEA) showed that NF-kappa B signaling pathway enriched
217 in *Prdm1*-deficient cNK cells (Figure 3D), suggesting the potential targets by *Prdm1* to regulate NK
218 cell function. Increased expression of multiple TFs such as *Junb*, *Batf3*, *Nfkb1*, *Tcf7*, and *Nr4a2* was
219 observed in *Prdm1* knockout cNK cells, suggesting they might be suppressed by *Prdm1* (Figure 3E).
220 Downregulation of granzyme B (*Gzmb*), Perfroin (*Prf1*) were observed in *Prdm1* deficient NK cells
221 (Figure 3E), implied decreased anti-tumor ability, which was consistent with increased melanoma

222 metastasis in *Prdm1*$^{\Delta Ncr1}$ mice (Figure 2, B and D). CXCR6 and CX3CR1 was considered to play
223 an important role in promoting the egress of NK cells from bone marrow. Decreased expression of
224 *Cxcr6* and *Cx3cr1* in *Prdm1*$^{\Delta Ncr1}$ NK (Figure 3E) might be the reason for the increased quantity of
225 NK cells in bone marrow and decreased number in peripheral tissues (Figure 1G). As a result of the
226 reduced expression levels of *Cxcr6* and *Cx3cr1*, NK cells may not be able to egress from the bone
227 marrow and accumulated therein. Consistent with decreased production of IFN-γ after stimulated
228 by IL-12/IL-18 (Figure 2F), decreased expression of *Il18rap* and *Il12rb2* were observed in
229 *Prdm1*$^{\Delta Ncr1}$ cNK cells (Figure 3E), implying impaired response to cytokine stimulation.

230 To confirm the result of RNA-sequencing, the expression of fractalkine receptor (CX3CR1),
231 granzyme B and perforin were analyzed by flow cytometry. The percentage of CX3CR1^{+} cNK cells
232 was significantly decreased in multiple tissues of *Prdm1*$^{\Delta Ncr1}$ mice, while the proportion of
233 CX3CR1^{+} ILC1 was increased in the liver (Figure 3, F and G). Lower GZMB and PRF1 production
234 was observed in *Prdm1*-deficient splenic cNK cells, liver cNK cells and ILC1s (Figure 3, H-K;
235 Supplemental Figure 4, A-I). Notably, the proportion of GZMB^{+} and PRF1^{+} cNK cells was
236 decreased among almost all of the maturation stages of cNK cells (Figure 3, J and K). The relative
237 mean fluorescent intensities (MFIs) of GZMB and PRF1 consistently show a reduction across all
238 developmental stages in *Prdm*$^{\Delta Ncr1}$ NK cells (Supplemental Figure 4, H and I). Yet, no statistical
239 difference of PRF1 was found within the CD11b^{-}CD27+ and CD11b^{+}CD27^{+} subsets, likely due to
240 the relatively lower perforin levels in these populations (Supplemental Figure 4I). These findings
241 suggest that Prdm1 may directly influence cytotoxic molecule in NK cells, rather than impacting
242 their anti-tumor abilities solely by affecting the maturation phenotype of Prdm1-deficient NK cells.

243 **scRNA-seq reveals distinct properties of two clusters from liver group I ILCs following *Prdm1***
244 **knockout**

245 To further investigate the effect of *Prdm1* in liver cNK cells and ILC1s and the changes in the
246 haptic immune microenvironment caused by the deficiency of *Prdm1* in group 1 ILCs, single-cell
247 RNA sequencing (scRNA-seq) was performed for liver $CD45^+$ cells (Figure 4A; Supplemental
248 Figure 5A). Initial quality control revealed high-quality of cell purity, library assembly, and
249 sequencing (Supplemental Figure 5B). 10978 cells passed the quality criteria and were selected for
250 further analysis (6,161 from *Prdm1*$^{+/+}$ mice, 4,817 from *Prdm1*$^{\Delta Ncr1}$ mice). Unsupervised clustering
251 of all sequenced cells based on transcript signatures identified twelve distinct clusters (Supplemental
252 Figure 5C), including B cells, epithelial cells (ECs), $CD4^+$ T cells, $CD8^+$ T cells, NKT cells, ILC1s,
253 cNK cells, dendritic cells (DCs), monocyte-derived macrophages (MDMs), Monocytes, Kupffer
254 cells (KCs), Neutrophils, and a small number of undefined cells (Figure 4A). In *Prdm1*$^{\Delta Ncr1}$ mice,
255 an increased proportion of MDMs, $CD4^+$ T cells, $CD8^+$ T cells, Monocytes, and DCs was observed,
256 alongside a decreased proportion of ECs, cNK cells, ILC1s, and NKT cells (Supplemental Figure
257 5D). Liver cNK cells and ILC1s were identified and discriminated based on the expression of
258 surface markers and distinctive TFs (Supplemental Figure 5, E and F). Compared with other clusters,
259 cNK cells and ILC1s highly expressed *Ncr1* and *Klrb1c* (NK1.1) (Supplemental Figure 5E). cNK
260 cells expressed high levels of *Itga2* (CD49b) and Eomes, while ILC1s had high levels expression
261 of *Itga1* (CD49a) and *Tnfsf10* (Supplemental Figure 5, F and G). Consistent with our flow cytometry
262 data, both cNK cells and ILC1s have significant reduced proportion in *Prdm1*$^{\Delta Ncr1}$ mouse
263 (Supplemental Figure 5H). In group 1 ILCs from *Prdm1*$^{\Delta Ncr1}$ mice, there was an increase in the
264 proportion of cNK cells accompanied by a decrease in ILC1s (Figure 4, B and C).

265 To better understand the specific function of *Prdm1* in liver cNK cells and ILC1s, the two
266 subpopulations of liver group 1 ILCs were further analyzed separately using unsupervised clustering
267 and visualized by Uniform Manifold Approximation and Projection (UMAP) (Figure 4, D and E).
268 Based on the cluster specific gene expression signature (Supplemental Figure 6A), the
269 subpopulation of liver cNK cells were referred as "*Prf1*^{hi}", "*Junb*^{hi}", and "*Cxcr3*^{hi}" cNK cells
270 (Figure 4D), with different distribution in *Prdm1*$^{\Delta Ncr1}$ and *Prdm1*$^{+/+}$ genotype (Figure 4F;
271 Supplemental Figure 6B).

272 The *Prf1*^{hi} cNK cell cluster was defined by high expression of cytolysis-related genes,
273 including *Ncr1*, *Gzma*, *Gzmb*, *Prf1*, and *Fgl2* (Figure 4G; Supplemental Figure 6, C and D),
274 indicating the strong target-killing ability of this cluster. Although this cluster is present in both
275 *Prdm1*$^{\Delta Ncr1}$ and *Prdm1*$^{+/+}$ mice, there is a significant reduction in *Prdm1*$^{\Delta Ncr1}$ mice (Figure 4F),
276 indicating the importance of Prdm1 in maintaining this group of cells. GO analysis further revealed
277 the enrichment signatures of cytolysis, response to virus, and lymphocyte mediated immunity in the
278 genes upregulated in *Prf1*^{hi} cNK cell cluster, further confirming the cytotoxic effects of this cluster
279 (Figure 4H). These data underscore the crucial role of *Prdm1* in maintaining NK cells with immune
280 effector functions.

281 The *Junb*^{hi} liver cNK cell cluster distinguished themselves by higher expression of *Junb*
282 compared to other clusters (Figure 4G; Supplemental Figure 6, C and D). The predominant majority
283 (92.98%) of *Junb*^{hi} liver cNK cells are derived from *Prdm1*$^{\Delta Ncr1}$ mice, with less than ten percent
284 (7.02%) originating from *Prdm1*$^{+/+}$ mice (Figure 4F). Many signal transduction elements, gene
285 expression regulator, and transcriptional factors, such as *Nfkbia*, *Tnfaip3*, *Nr4a1/2/3*, *Batf3*, *Fos*,
286 *Fosb*, *Tcf7*, and *Kit* were upregulated in the *Junb*^{hi} liver cNK cells (Figure 4G; Supplemental Figure

287 6D). The expression of cytotoxicity related genes, such as *Gzmb* and *Prf1*, in *Junb*^{hi} cluster was also
288 lower than other cNK cell clusters (Figure 4G). GO analysis showed that the genes upregulated in
289 *Junb*^{hi} liver cNK cells enriched in cell differentiation, cell activation, and transcriptional regulation
290 (Figure 4H). GSEA indicates that the NF-kappa B, IL-17, MAPK, and TNF signaling pathways
291 were upregulated in this clusters (Figure 4, I-L). GSEA also showed that mitochondrial related
292 pathways, such as mitochondrial protein, oxidative phosphorylation, and respiratory electron
293 transport chain were suppressed in *Junb*^{hi} cNK cell cluster (Supplemental Figure 6, E-G). Increased
294 proportion of *Junb*^{hi} cluster in *Prdm1* deficient cNK cells suggested impaired anti-tumor activity,
295 which was consistent with more melanoma metastasis in *Prdm1*$^{\Delta Ncr1}$ mice and lower expression of
296 cytotoxicity-related genes in splenic cNK cells based on bulk RNA-sequencing.

297 The *Cxcr3*^{hi} cNK cell cluster was characterized with high expression of *Cxcr3*, *Ccr2*, and some
298 genes encoding ribosomal subunits such as *Rps7* (Supplemental Figure 6A). Expression of tissue-
299 resident markers Cd69 was also highly expressed in this clusters (Supplemental Figure 6D). The
300 enrichment of chemokine receptors in the genes upregulated in the *Cxcr3*^{hi} cluster implying a greater
301 likelihood of this cluster being tissue-resident compared with other cNK cell clusters (Figure 4H).
302 To further confirmed tissue-resident properties of this clusters, we calculated the module score based
303 on top30 DEGs in ILC1 versus cNK clusters, including *Cxcr6*, *Itga1*, *Cd160*, *Cd226*, etc. *Cxcr3*^{hi}
304 cNK clusters have the highest score among all cNK clusters (Supplemental Figure 6H), indicating
305 the similarity with liver ILC1s. In the tumor microenvironment, reports indicated that NK cells
306 could transform into ILC1s (24). If this conversion of cNK cells into ILC1s also occurred under
307 normal physiological conditions, then *Cxcr3*^{hi} cNK cell cluster might be the most susceptible to
308 such transformation.

309 The significant enrichment of ribosomal subunits and cytoplasmic translation in *Cxcr3*^{hi} cluster
310 (Figure 4H) implied their distinct and active metabolic profile and the capability to mount immune
311 responses. The remarkably decreased proportion of *Cxcr3*^{hi} cNK cell cluster in *Prdm1*$^{\Delta Ncr1}$ mice
312 (Figure 4F), which emphasized the critical role of *Prdm1* in maintaining this cluster of liver cNK
313 cells, consistent with the flow cytometry result that showed an increase in the number of NK cells
314 in the bone marrow and a decrease in NK cells in peripheral tissues (Figure 1G). To confirm the
315 regulatory effect of Prdm1 on the migration of NK cells and ILC1 through chemokine receptors,
316 and to validate the scRNA-seq data, we further evaluated the expression of CX3CR1 by flow
317 cytometry. A decrease in the proportion of CX3CR1^{+} NK cells was observed across all tested organs
318 following Prdm1 knockout. However, it is noteworthy that, in contrast to the trend in NK cells,
319 CX3CR1 expression was increased in liver ILC1s after Prdm1 knockout (Figure 3, F and G). This
320 not only substantiates the involvement of Prdm1 in managing NK cell migration but also
321 underscores its distinctive regulatory impacts on the chemokine receptor expressions within NK
322 cells and ILC1 populations. Bulk RNA sequencing data also found that the expression of *Cx3cr1*
323 and *Cxcr6* decreased in *Prdm1*$^{\Delta Ncr1}$ cNK cells (Figure 3E). These findings supported the hypothesis
324 that *Prdm1*, through regulating chemokine receptor expression levels, influenced the distribution of
325 NK cells in the bone marrow and peripheral tissues, particularly within the liver tissue.

326 Three clusters of ILC1s were identified from liver ILC1s (Figure 5A), comprising "*Il7r*^{hi}",
327 "*Klra*^{hi}", and "*Gzmb*^{hi}" ILC1s. *Prdm1*$^{+/+}$ and *Prdm1*$^{\Delta Ncr1}$ ILC1s seemed to co-cluster largely and
328 have minor difference within the proportion of clusters (Figure 5, B and C; Supplemental Figure
329 7B). The first two clusters of ILC1s were characterized by higher expression of *Il7r* (CD127) and
330 *Klra5* separately, while the *Gzmb*^{hi} ILC1 cluster was identified by elevated expression of both *Gzma*

331 and *Gzmb* (Figure 5D; Supplemental Figure 7, A, C and D). Additionally, both *Gzma* and *Gzmb*
332 expression were downregulated, and *Junb* was upregulated, in *Prdm1*$^{\Delta Ncr1}$ mice derived cNK cells
333 and ILC1s compared to those from *Prdm1*$^{+/+}$ mice (Figure 5E). The *Il7r*^{hi} ILC1s cluster was
334 distinguishable from other ILC1 clusters by its high expression of *Il7r*, IL18RA (*Il18r1*), and IFN-
335 γ (*Ifng*) (Figure 5B; Supplemental Figure 7C). The high expression of *Il18r1* and *Ifng* in *Il7r*^{hi} ILC1s
336 indicated this cluster of cells was highly responsive to IL-18 (Supplemental Figure 7D). GSEA and
337 GO analysis showed that IL-17, NF-kappa B, TNF, MAPK signaling pathway and T cell
338 differentiation were activated in the *Il7r*^{hi} ILC1 cluster (Figure 5, F-H; Supplemental Figure 7, E-
339 G). Module scores, calculated based on the expression of feature genes within the *Junb*^{hi} cNK cell
340 cluster, revealed a comparable *Junb*^{hi} signature expression pattern within the *Il7r*^{hi} ILC1 cluster
341 (Figure 5I). Several ILC3 signature genes, such as *Rora*, *Tmem176a,* and *Tmem176b* (44), highly
342 expressed in this cluster (Supplemental Figure 7D). Considering the close relationship between IL-
343 17 mediated immunity response and ILC3 (1, 45), it is plausible that *Il7r*^{hi} ILC1 cluster may be
344 attributed, at least in part, to potential plasticity between ILC1 and ILC3 subsets.

345 The second liver ILC1 cluster, characterized by high expression of Ly49E (*Klra5*) and Ly49G
346 (*Klra7*), was designated as the *Klra*^{hi} ILC1 cluster (Figure 5D; Supplemental Figure 7D). Notably,
347 there was an elevated proportion of *Klra*^{hi} ILC1s in *Prdm1*$^{\Delta Ncr1}$ ILC1s (39.7%) compared to
348 *Prdm1*$^{+/+}$ ILC1s (28.1%) (Figure 5C). Liver Ly49E^{+} ILC1s have been identified as possessing
349 greater cytotoxic potential and a more robust viral response compared to liver Ly49E^{-} ILC1s (46).
350 The *Klra*^{hi} cluster exhibited notably high expression of *Ccl5* (Supplemental Figure 7D). Previous
351 research has underscored the pivotal role of CCL5, produced by both cNK cells and ILC1s, in
352 facilitating the accumulation of DCs within the tumor microenvironment, thereby impeding tumor

353 immune evasion, as highlighted in studies (47, 48). The expression of *Ccl5* was reduced in the *Klra*^{hi}

354 cluster of *Prdm1*$^{\Delta Ncr1}$ ILC1s compared to *Prdm1*$^{+/+}$ ILC1s (Supplemental Figure 7D), which could

355 potentially have a detrimental impact on the ability of *Klra*^{hi} ILC1s to develop a connection between

356 innate and adaptive immune responses.

357 The *Gzmb*^{hi} ILC1 cluster was identified according to the high expression of *Gzma*, *Gzmb*, and

358 *Fgl2* (Supplemental Figure 7D) compared to other ILC1 clusters. GO analysis also revealed the

359 enrichment in cytolysis and stimulus-response capacity (Figure 5H) of the *Gzmb*^{hi} ILC1 cluster.

360 Consistent with the *Prf1*^{hi} cNK cell cluster, the proportion of the *Gzmb*^{hi} cluster among liver ILC1s

361 exhibited a considerable reduction in *Prdm1*$^{\Delta Ncr1}$ mice compared to *Prdm1*$^{+/+}$ mice, and the

362 expression of *Gzma* also downregulated in *Prdm1*$^{\Delta Ncr1}$ mice (Figure 5B). Previous reports showed

363 that GzmA^{+} ILC1 constituted the main population of liver ILC1s at birth, with the potential target-

364 killing ability (49, 50). Within cNK cells, *Il12rb2*, *Il18r1* and *Il18rap* was highly expressed in *Prf1*^{hi}

365 and *Cxcr3*^{hi} cNK clusters (Supplemental Figure 6I), indicating the IL-18 receptor expression

366 correlated with the NK cell maturation. While in ILC1, these receptors mostly expressed on *Il7r*^{hi}

367 and *Gzmb*^{hi} ILC1 clusters (Supplemental Figure 7D). Significant decreased of *Il18r1* expression in

368 *Prdm1*$^{\Delta Ncr1}$ cNK cells and ILC1s may associated with the impaired ability to produce IFN-γ.

369 To investigate the universal transcriptional program between group 1 ILCs across liver and

370 spleen, we have explored DEGs in *Prdm1*$^{\Delta Ncr1}$ liver cNK cells and ILC1s using our scRNA-seq data.

371 Compared with liver ILC1s, more valuable DEGs was observed in liver cNK cells, including *Junb*,

372 *Kit*, *Tcf7*, *Gzmb*, *Prf1*, etc. (Supplemental Figure 8, A and B). Through the integration of the bulk

373 RNA-seq and scRNA-seq data, we identified 17 DEGs that are regulated by Prdm1 among liver

374 cNK cells, splenic cNK cells, and liver ILC1s. *Batf3*, *Junb*, *Tcf7*, and *Nfkb1* was upregulated,

375 whereas *Gzmb*, *Prf1*, and *Fgl2* downregulated, in both *Prdm1*$^{\Delta Ncr1}$ liver and splenic cNK cells
376 (Figure 5J). Cxcr6 was downregulated in liver ILC1s and splenic cNK cells in *Prdm1*$^{\Delta Ncr1}$ mice
377 (Figure 5J). Previous research found that spleen NK cells could be divided into three distinct groups
378 based on their expression levels of CD27, CD62L, CD49a, and CD49b (51). CD27^{+}CD62L^{-} NK
379 cells have remarkable high expression of Batf3, while it was only barely expressed in
380 CD27^{+}CD62L^{+} and CD27^{-}CD62L^{+} NK cells (51). Based the sequencing data published by
381 Flommersfeld et al., (GSE180978), a notable negative correlation was observed between the
382 expression levels of Prdm1 and Batf3 (Supplemental Figure 8I). On top of that, our findings
383 unveiled the negative regulatory influence of Prdm1 on Batf3 within both spleen and liver NK cells.
384 This discovery highlights a potential upstream mechanism that may influence the hemostasis of the
385 spleen NK cell subpopulations through Batf3.

386 We also compared the gene expression patterns between *Prdm1* and *Hobit* (homologue of
387 Blimp1) with two published scRNA-seq data (50, 52). Following the knockout of Hobit, the DEGs
388 were primarily identified within ILC1s. Conversely, after the knockout of Prdm1, a greater number
389 of DEGs were observed in cNK cells. This indicates that Prdm1 likely possesses a broader range of
390 target genes within cNK cells, whereas Hobit appears to have a more pronounced impact on gene
391 expression within ILC1s (Supplemental Figure 8, C-F). There are some overlaps between the
392 downstream transcriptional profile of *Prdm1* and *Hobit* in liver cNK cells and ILC1s (Supplemental
393 Figure 8, G and H), such as *Junb*, *Fosb*, *Tcf7*, *Kit*, *Gzmb*, *Prf1*, and *Cxcr6* was simultaneously
394 upregulated or downregulated in both *Prdm1*$^{\Delta Ncr1}$ and *Hobit*^{KO} liver cNK cells or ILC1s, indicating
395 the similar regulatory networks of Prdm1 and Hobit.

396 ***Prdm1* facilitates the intercellular communication between liver group 1 ILCs and**

397 **macrophages**

398 The reciprocal crosstalk between group 1 ILCs and macrophages plays a critical role in

399 maintaining liver immune homeostasis and anti-cancer immune surveillance (53, 54). The scRNA

400 sequencing analysis identified two well-established subpopulations of liver macrophages: the

401 resident Kupffer Cells (KCs) and the Monocyte-Derived Macrophages (MDMs) (Figure 6, A-C;

402 Supplemental Figure 9A). When comparing the total proportion of macrophages within the immune

403 cell population of the liver between WT and *Prdm1*$^{\Delta Ncr1}$ mice, there is an increase in *Prdm1*$^{\Delta Ncr1}$

404 mice (Figure 6C). To confirm these findings, we utilized flow cytometry to define macrophages,

405 including both KCs and MDMs, gating by CD45^{+}Ly6G^{-}F4/80^{+}CD11b^{+} (Figure 6D). Our analysis

406 showed that, following the deletion of *Prdm1* in Group 1 ILCs, there is a significant increase in both

407 the proportion and number of macrophages in the liver (Figure 6D).

408 According to the transcriptional profile, liver macrophages further clustered and were labeled

409 as "*Ly6c2*^{hi}"; "*Cxcl2*^{hi}"; "*Ear2*^{hi}" MDMs, and "*Mrc1*^{hi}"; "*C1q*^{hi}" KCs (Figure 6A, Supplemental

410 Figure 9, A-E). Increased proportion of MDMs and KCs was observed in *Prdm1*$^{\Delta Ncr1}$ cells

411 (Supplemental Figure 9B). Within MDMs clusters, *Ly6c2*^{hi} MDMs mainly compose of *Prdm1*$^{+/+}$

412 cells, while *Prdm1*$^{\Delta Ncr1}$ cells concentrated in *Cxcl2*^{hi} cluster (Figure 6C). The scRNA-seq data reveal

413 that following Prdm1 knockout in NKp46^{+} cells, there is a decrease in the proportion of KCs within

414 the macrophage population, while the proportion of MDMs increases (Figure 6D). CX3CR1, a

415 chemokine receptor, is extensively utilized to distinguish KCs and MDMs within macrophages.

416 Cells expressing CX3CR1 are identified as MDMs, whereas those without CX3CR1 expression are

417 categorized as KCs (55). Employing flow cytometry and leveraging CX3CR1 expression, we

418 assessed the ratios of KCs and MDMs. However, diverging from the scRNA-seq findings, flow
419 cytometry indicates that post-Prdm1 knockout in group 1 ILCs, there is a minor increase in the
420 proportion of KCs within the total liver macrophages, and a decrease in the proportion of MDMs
421 (Figure 6D; Supplemental Figure 9B). This discrepancy could stem from the different bases of
422 classification: scRNA-seq defines KCs based on gene expression profiles, whereas flow cytometry
423 differentiates between KCs and MDMs using the single surface marker, CX3CR1. Analysis of the
424 macrophage subsets identified by scRNA-seq reveals that, while MDM clusters generally show high
425 CX3CR1 expression, there exists a subset within MDMs, labeled *Mrc1*^{hi}, that also exhibits high
426 levels of CX3CR1 (Supplemental Figure 9C). Consequently, if flow cytometry solely employs
427 CX3CR1 for differentiating between KCs and MDMs, it could result in disparities when compared
428 to scRNA-seq outcomes. Both KCs and MDMs has significantly increased in *Prdm1*$^{\Delta Ncr1}$ mice,
429 which was consist with the scRNA-seq data (Supplemental Figure 9, B and F). Despite the decrease
430 in the proportion of *Ly6c2*^{hi} MDMs in *Prdm1*$^{\Delta Ncr1}$ mice, the expression levels of *Ly6c2* exhibited
431 minimal variation between WT and *Prdm1*$^{\Delta Ncr1}$ mice (Supplemental Figure 9D). Intriguingly, within
432 certain cellular subsets, notably the *Ear2*^{hi} cluster, the *Ly6c2* expression levels in KO mice were
433 found to be higher than those in WT mice. Additionally, we employed flow cytometry to examine
434 Ly6C expression within the macrophages. Similar with the scRNA-seq findings, there were no
435 notable differences in Ly6C expression levels between WT and KO mice (Figure 6E; Supplemental
436 Figure 9G).

437 High-resolution interactions among liver cNK cells, ILC1s, and macrophages were established
438 and compared between *Prdm1*$^{+/+}$ and *Prdm1*$^{\Delta Ncr1}$ mice using the CellChat program (56). Interactions
439 between ILC1s and total macrophages were higher than that between cNK cells and macrophages

440 (Supplemental Figure 10, A, C, E, and G). Cross-talk between liver group 1 ILCs with macrophages
441 enriched in macrophage migration inhibitory factor (MIF), MHC-I, CXC chemokine ligand (CXCL),
442 Thy-1 cell surface antigen (THY1), and C-type lectin (CLEC) pathways (Supplemental Figure 10,
443 B, D, F, and H). Although the quantity of macrophages significantly increases in *Prdm1*$^{\Delta Ncr1}$ mice,
444 there is a significant decrease in the interaction number and interaction strength between liver group
445 1 ILCs and macrophages (~1.5 fold) in *Prdm1*$^{\Delta Ncr1}$ mice (Figure 6, F and G). The reduction of
446 interaction mostly occurred in the cross-talk of ILC1-MDM and ILC1-KC, whereas no difference
447 was observed in cNK-MDM and cNK-KC interaction (Supplemental Figure 10, A-H). A reduction
448 in the interaction of ligand-receptor, such as Mif-CD74, Cxcl16-Cxcr6, and Cxcl10-Cxcr3 was
449 observed in *Prdm1*$^{\Delta Ncr1}$ mice compared to *Prdm1*$^{+/+}$ mice (Supplemental Figure 11). Compared to
450 *Prdm1*$^{+/+}$ mice, the information flow of CXCL and MIF pathways significantly decreased in
451 *Prdm1*$^{\Delta Ncr1}$ mice (Figure 6, H and I; Supplemental Figure 10, B, D, F, and H). These pathways play
452 a crucial role in facilitating macrophage migration. The CXCL signaling was sent from *Ly6c2*^{hi}
453 *Cxcl2*^{hi} MDMs and *C1q*^{hi} KC, targeting all ILC1 clusters and *Cxcr3*^{hi} cNK cell clusters (Figure 6J).
454 Of note, although the population of *Cxcl2*^{hi} macrophage primarily comprised cells from *Prdm1*$^{\Delta Ncr1}$
455 mice, the interaction within the CXCL pathway between macrophages and group 1 ILCs was
456 obviously less than *Prdm1*$^{+/+}$ sample (Figure 6J). These changes could be linked to a decreased
457 population of ILC1s and *Cxcr3*^{hi} cNK cell cluster in *Prdm1*$^{\Delta Ncr1}$ mice, implying that the homeostasis
458 of *Cxcl2*^{hi} macrophages required sufficient signals from cNK cells and ILC1s. The impaired CXCL-
459 CXCR interactions might subsequently lead to reduced recruitment and activation of group 1 ILCs
460 and macrophages within the tumor microenvironment.

461 ***Prdm1* safeguards group 1 ILCs from exhaustion-like phenotypes in the tumor**
462 **microenvironment**

463 The suppression of mitochondrial related pathways in *Junb*^{hi} cNK cell cluster, along with a
464 significant increase of this cNK cell cluster in *Prdm1*$^{\Delta Ncr1}$ mice, encouraged us to explore
465 mitochondrial function through flow cytometry. MitoTracker, MitoSOX, and
466 Tetramethylrhodamine methyl ester (TMRM) were used to assess the mitochondrial mass,
467 superoxide production, and mitochondrial membrane potential. A substantial decrease in MFIs of
468 MitoTracker was observed in *Prdm1*$^{\Delta Ncr1}$ splenic cNK cells, liver cNK cells, and liver ILC1s when
469 compared to their *Prdm1*$^{+/+}$ counterparts (Figure 7A). This observation aligns with the enrichment
470 of downregulated genes from *Prdm1* deficient sample in mitochondrial related pathway, as revealed
471 by RNA sequencing data (Supplemental Figure 6, D-F). There was no significant difference in
472 MitoSOX and TMRM between *Prdm1*$^{\Delta Ncr1}$ and *Prdm1*$^{+/+}$ mice (Figure 7, B and C), which suggested
473 that the ATP synthesize capacity was minimally affected by *Prdm1*.

474 IFN-γ is a critical cytokine for NK cells mediated cancer surveillance(57, 58) and impaired
475 production of IFN-γ was considered as a key hallmark of exhausted NK cells (59, 60). To evaluate
476 the IFN-γ secreting capacity of liver cNK cells and ILC1s in tumor microenvironment, B16F10
477 tumor cells were inoculated to the liver via splenic injection and the IFN-γ levels in response to
478 stimulation of IL-12 and/or IL-18 were assessed by flow cytometry (Supplemental Figure 12A).
479 The proportion changes of cNK cells and ILC1s in *Prdm1*$^{\Delta Ncr1}$ mice was similar with the no tumor-
480 burden condition, while the number of both cNK cells and ILC1s have significant decreased in
481 tumor-bearing liver (Figure 7D). Compared with *Prdm1*$^{+/+}$ mice, significant deceased of IFN-γ were
482 observed in *Prdm1*$^{\Delta Ncr1}$ mice liver cNK cells and ILC1s under the combinate stimulation of IL-

483 12/IL-18 (Figure 7E; Supplemental Figure 12B), which was more remarkable in liver ILC1s. Similar
484 trends were observed when IL-12 or IL-18 was used alone, although only liver ILC1s showed a
485 significant decrease in response to IL-18 stimulation (Figure 7E). These findings were consistent
486 with the heavy tumor burden observed in *Prdm1*$^{\Delta Ncr1}$ mice.

487 **Discussion**

488 Prdm1 is a pivotal transcription factor that has attracted substantial research interest due to its
489 role in lymphocytes. In a study involving systemic knockout combined with competitive
490 transplantation, it was found that Prdm1 promotes NK cell maturation and the expression of Gzmb.
491 On the contrary, the same study also found that NK cells with Prdm1 deficiency exhibit heightened
492 proliferation, increased survival, enhanced migratory abilities towards tumors, and greater
493 cytotoxicity against subcutaneously implanted RMAS tumors (30). Using Ncr1-driven conditional
494 knockout transgenic mice, which specifically delete *Prdm1* in group 1 ILCs, we not only validated
495 *Prdm1*'s positive regulation of NK cell maturation, but also demonstrated its indispensable role in
496 NK cell anti-tumor activity. The compromised mitochondrial function and reduced IFN-γ, granzyme
497 B, and perforin production appear to be potential contributing factors to Prdm1-mediated cancer
498 surveillance. Reduction of CX3CR1^{+} NK cells in multiple tissues, and decreased expression of
499 *Cx3cr1* and *Cxcr6* was observed in *Prdm1*$^{\Delta Ncr1}$ splenic cNK cells (Figure 3F), both of which are
500 essential for NK cells egressing from bone marrow (61, 62). Our results not only confirmed a
501 decrease in cytotoxic molecules in *Prdm1*-deficient NK cells (30) but also showed that the reduction
502 in Gzmb and perforin is not solely attributable to the diminished maturation of these cells. Mature
503 NK cells in bone marrow obtained the expression of CX3CR1 and acquired ability to enter the

504 circulation (61, 62). The quantity of cNK cells increased exclusively in the bone marrow, with
505 reductions observed in all other tissues (Figure 1G), indicating *Prdm1* might regulate chemokine
506 receptors to facilitate the egression of cNK cells from the bone marrow to peripheral tissues. In
507 addition, higher expression of *Cxcr6* compared to cNK cells is also a key factor for liver tissue
508 residence of ILC1s (63). Decreased expression of *Cxcr6* in *Prdm1* deficient group 1 ILCs may also
509 contribute to the balance shift towards cNK cells. Furthermore, although both liver NK cells and
510 liver ILC1s require Prdm1 to maintain their quantity, liver ILC1s demonstrate a more pronounced
511 dependency on Prdm1. However, it is currently widely believed that liver NK cells and liver ILC1s
512 originate from different progenitors. It is worth noting that while we observed changes in the NK
513 and ILC1 proportions after *Prdm1* knockout, our data does not support the hypothesis that Prdm1
514 affects progenitor differentiation decisions, thereby influencing the fate selection of NK and ILC1.
515 Further research may be needed to elucidate how Prdm1 regulates the balance between NK cells
516 and ILC1s.

517 scRNA sequencing analysis reveals that both liver cNK cells and ILC1s can be further divided
518 into three subgroups based on their gene expression patterns. Junb is a crucial transcriptional factor
519 for the cytotoxic function of $CD8^+$ T cells and NK cells. However, excessive *Junb* expression has
520 been found to promote T cell exhaustion (64). Our previous study showed that as NK cells mature,
521 the expression level of *Prdm1* increased while the expression level of *Junb* gradually decreased (25).
522 The current study demonstrated that in NK cells, the expression level of *Junb* significantly increases
523 upon the deletion of Prdm1, indicating that *Junb* expression is suppressed by Prdm1. As *Junb*
524 expression decreases with NK cell maturation, and it is inhibited by the gradually increasing Prdm1
525 during maturation. This implies that constraining *Junb* expression is likely a fundamental

526 prerequisite for NK cell maturation. However, the precise mechanism by which Prdm1
527 downregulates *Junb* in NK cells still needs further research. Furthermore, *Junb*^{hi} NK cells exhibit
528 lower expression levels of cytotoxic genes and reduced mitochondrial-related signaling pathways.
529 Mitochondria are pivotal organelles crucial for cellular metabolism. Disruptions in mitochondrial
530 function have been linked to T Cell exhaustion, attributed to glycolytic reprogramming (65).
531 Similarly, mitochondrial fragmentation has been closely associated with NK cell exhaustion (66).
532 However, the concept of NK cell exhaustion isn't as firmly established as it is for T cells. Exhausted
533 NK cells should primarily exhibit diminished functions. This is characterized by a diminished ability
534 to destroy tumor cells, a reduced capability to activate other components of the immune system, and
535 compromised proliferation and survival rates. Additionally, this reduced functionality is associated
536 with a decline in the expression of molecules responsible for cytotoxic activity, lower production of
537 IFN-γ, and metabolic disturbances that may arise from mitochondrial dysfunction. While our current
538 data is not sufficient to definitively classify these cells as exhausted NK cells, it supports that a
539 subpopulation, referred to *Junb*^{hi} cluster, demonstrates an exhaustion-like phenotype. The
540 significant increase in this cell population following *Prdm1* knockout in NK cells may potentially
541 be one of the reasons why *Prdm1*$^{\Delta Ncr1}$ mice lose their tumor-killing capacity. Whether the excessive
542 expression of JunB in NK cells is also a contributing factor to their exhaustion, similar to T cells(64),
543 requires further investigation.

544 The scRNA-seq data revealed that *Prdm1* plays distinct roles in regulating cNK cells and ILC1s
545 despite being required for the quantity of both lineages. Specifically, *Prdm1* appears to be more
546 involved in promoting the resistance against exhaustion in cNK cells, whereas in ILC1s, it may play
547 a role in the plasticity between ILC1s and ILC3s. In both our previous study and a study by Colonna

548 et al. (25, 67), it was demonstrated that *Smad4*, a transcriptional factor involved in TGF-β signal
549 pathway, upregulated *Prdm1* in NK cells and depletion of *Smad4* resulted in a decreased ratio of
550 NK cells to ILC1s in the liver. However, knocking out *Prdm1* in Ncr1^{+} cells increased the ratio of
551 NK cells to ILC1s in liver group 1 ILCs (Figure 2A). These findings suggest the possibility of a
552 Smad4-independent pathway through which *Prdm1* promotes the maintenance of ILC1s, or that
553 *Prdm1* plays a more significant role in maintaining ILC1s compared to its role in NK cells.

554 Previous studies have identified Hobit and Prdm1 as central regulators instructing tissue-
555 dependent programs and retention of diverse tissue-resident lymphocytes (17, 50, 52). Liver ILC1s
556 required Hobit, but not necessary for cNK cells (6). Expression of Prdm1 was remarkably higher in
557 cNK cells versus ILC1s (17). While in our study, cNK cells and liver ILC1s reduced simultaneously
558 in *Prdm1*$^{\Delta Ncr1}$ mice, and even more significant in ILC1s. This indicates that while Prdm1 is
559 expressed at lower levels in ILC1s, its role in preserving the quantity of ILC1s may be more crucial.
560 Thus, Prdm1 and Hobit may have parallel program in instructing ILC1s functional development and
561 maturation. Prdm1 and Hobit directly bound and repressed *Tcf7* (17), which encoded TCF-1, a TF
562 binding and limiting the activity of Gzmb regulatory element (68). Gzmb has been demonstrated
563 directly bound and activated by Junb in NK cells, which suggested Gzmb expression regulated by
564 multiple Prdm1/Hobit downstream signals (25). In human T cells, binding motif of JUNB was
565 enriched in the binding sites of PRDM1 (69), indicating the essential role of PRDM1-JUNB axis
566 during NK cell and T cell development. In NK cells deficient in Prdm1 expression, we noted a
567 decrease in Gzmb levels alongside with an elevation in Junb expression. This indicates that Prdm1
568 not only facilitates the expression of Gzmb in NK cells but also suppresses Junb expression. Given
569 that Junb is recognized as a positive regulator of Gzmb (70), this presents a complex interplay that

570 seems contradictory. Therefore, it is imperative to develop a theoretical framework to
571 comprehensively understand and interpret this paradoxical relationship. Our previous research has
572 demonstrated that with the progression of NK cell maturation, there is a gradual increase in Prdm1
573 expression, accompanied by a subtle reduction in JunB levels (25). Overexpression of JunB can
574 induce lymphocyte exhaustion (64). Based on these findings, we hypothesize that during the initial
575 stages of NK cell development, JunB might enhance the expression of certain molecules associated
576 with cytotoxicity, thereby aiding NK cells in acquiring the capacity to eliminate target cells. During
577 these initial stages, Prdm1 level are comparatively low, thus exerting a weaker inhibitory effect on
578 JunB. As NK cells proceed to maturity, there's a progressive increase in Prdm1 level, which then
579 exerts a stronger inhibitory influence on JunB, contributing to the reduced JunB level in terminal
580 matured NK cells. Consequently, this reduces the potential for NK cell exhaustion caused by
581 elevated levels of JunB.

582 Chronic inflammation is a crucial factor in promoting tumorigenesis, and macrophages play a
583 significant role in this process. Macrophages interact with both cNK cells and ILC1s. However, the
584 TFs that regulate these interactions are poorly understood. Fortunately, recent advances in scRNA-
585 seq technology and the CellChat software tool (56) have allowed us to gain a better understanding
586 of the *Prdm1* signaling pathway in group 1 ILCs and its impact on macrophages at the transcriptional
587 level. Increased metastasis in *Prdm1*$^{\Delta Ncr1}$ mice may be due to a decrease in the killing ability of NK
588 cells, making them more prone to exhaustion, or it could be due to abnormalities in group 1 ILCs,
589 leading to a decrease in the anti-tumor abilities of macrophages and an enhancement of their pro-
590 tumor capabilities. It is worth noting that normal ILC1-macrophage interactions are more prevalent
591 than the interaction between NK cells and macrophages (Supplemental Figure 10). We also found

592 that CXCL signaling based interaction remarkably diminished in *Prdm1*$^{\Delta Ncr1}$ mice, which suggested
593 CXCL-CXCR may contribute to keep the sufficient interaction between group 1 ILC and
594 macrophage. Specifically, *Prdm1* in group 1ILCs may be critical in preventing the overactivation of
595 macrophages that can lead to cancer development. Increased population of both MDMs and KCs in
596 *Prdm1*$^{\Delta Ncr1}$ mice, as well as different distribution of macrophage clusters, indicating the homeostasis
597 of macrophages require environment with functional cNK cells and ILC1s. Although not all
598 macrophage phenotypes have been verified in this study, the present research serves primarily to
599 offer initial insights and preliminary data for investigating the interactions between group 1 ILCs
600 and macrophages. It aims to inspire further research into the role of transcription factors within the
601 liver and the cancer microenvironment.

602 While our findings underscore the importance of Prdm1 in liver cNK cells and ILC1s tumor
603 immune surveillance, it does not be validated in human NK cells, whereas previous studies have
604 found that PRDM1 might inhibit the proliferation and function of human NK cells (32, 71).
605 Furthermore, we not provided an in-depth evaluation in multiple tumor models. Further research
606 may provide deeper insight into the role of PRDM1 in the anti-tumor function of human NK cells,
607 enabling a more direct investigation of its application in cancer therapies. Given its important role
608 in preserving liver cNK cells and ILC1s functional heterogeneity, enhancing Prdm1 function in
609 human NK cells could potentially be a strategy to promote NK cell-based immunotherapy for cancer.

610 **Methods**

611 **Mice**

612 *Prdm1*$^{fl/fl}$ mice were purchased from The Jackson Laboratory. *Ncr1-iCre* and *B2m*$^{-/-}$ mice were

613 purchased from Shanghai Model Organisms Center, Inc.. Six- to twelve-week-old littermates were
614 used for the experiment.

615 **Experimental metastasis model**

616 For lung metastasis model, 0.3 × 10^6 B16F10 cells were intravenous injected into mice. Three
617 weeks later, mice were euthanized for analysis. For liver metastasis model, mice were inoculation
618 with 0.5 × 10^6 B16F10 via intrasplenic injection. Three weeks later, mice were euthanized for
619 analysis. Lung and liver from tumor-bearing mice were fixed in 10% formalin and embedded in
620 paraffin. Sections were stained with H&E.

621 ***In vivo* cytotoxicity assay**

622 Donor splenocytes harvested from B2m deficient ($B2m^{-/-}$) mice were labeled with 5 μM CFDA-
623 SE. Donor splenocytes harvested from B2m-adequate ($B2m^{+/+}$) mice were labeled with 5 μM eF670.
624 Labeled splenocytes from two mouse strains were mixed in a 1:1 ratio, and 1 × 10^7 cells in total
625 were injected i.v. into $Prdm1^{+/+}$ and $Prdm1^{\Delta Ncr1}$ mice. One day after administration, spleen and liver
626 cells were isolated from recipient mice, and the population of labeled cells was analyzed by flow
627 cytometry. Rejection % was quantified according to the following formula:
628 $1-(\%B2m^{+/+}/\%B2m^{-/-})_{Prdm1^{+/+}\text{ or }Prdm1^{\Delta Ncr1}}\times 100\%$.

629 **Cell isolation**

630 Mice were perfused with 1◊ PBS by portal vein puncture before harvesting tissues. Liver and
631 lung was digested with 0.05% collagenase II for 30 minutes and filtered through 70 μm cell strainers,
632 and mononuclear cells were isolated after subjected to density gradient using 30% and 70% percoll.

633 Spleen were also removed and pressed through 70 μm filterers to obtain splenocytes. Peripheral
634 blood mononuclear cells were obtained from peripheral blood after lysis of red blood cells
635 (Biolegend, 420301). Flushing femurs and mechanical disruption of inguinal lymph nodes were
636 performed to obtain cells from bone marrow and lymph nodes.

637 **Real-time RT-PCR**

638 RNA was extracted from FACS-sorted NK cells or splenocytes using RNASimple Total RNA
639 Kit (TIANGEN Biotech, 4992858) and subsequently reverse transcribed to cDNA with
640 SuperScript VILO Master Mix (Thermo Fisher Scientific, 11755050) according to manufacturer's
641 instructions. qPCR was performed with SYBR Green Mix (Thermo Fisher Scientific, A25742) and
642 CFX Opus 96 Real-Time PCR System (Bio-Rad). The relative mRNA expression level was
643 calculated using 2^{-ddCt} method. Primer sequences: *Prdm1*: 5'-CAGAAACACTACTTGGTACA-3';
644 5'-GATTGCTTGTGCTGCTAA-3'.

645 **Flow cytometry**

646 Flow cytometry and cell sorting were performed with a Cytoflex S/SRT (Beckman Coulter).
647 The following antibodies were used (all purchased from BioLegend unless otherwise indicated):
648 CD45-PE-Cy7 (catalog 103114, clone 30-F11); CD3ε-PerCP-Cy5.5 (catalog 100327, clone 145-
649 2C11); NK1.1-BV421 (catalog 108741, clone PK136); CD335-AF647 (catalog 560755, clone
650 29A1.4, BD Bioscience); CD49a-PE (catalog 562115, clone Ha31/8, BD Bioscience); CD49b-FITC
651 (catalog 108906, clone DX5); CD27-BV510 (catalog 124229, clone LG.3A10); CD11b-AF700
652 (catalog 101222, clone M1/70); KLRG1-APC (catalog 561620, clone 2F1, BD Bioscience); CD49a-

653 BV421 (catalog 740046, clone Ha31/8, BD Bioscience); IFN-γ-PE (catalog 505807, clone
654 XMG1.2); Granzyme B (catalog 372207, clone QA16A02); Perforin (catalog 154305, clone
655 S16009A); CD49b-APC-Cy7 (catalog 108919, clone DX5) ; IgG-PE (catalog 402203, clone 27-35);
656 CD335-BV510 (catalog 137623, clone 29A1.4);; CD3ε-APC-Cy7 (catalog 100330, clone 145-
657 2C11); CD11b-BV421 (catalog 101235, clone M1/70); CD3ε-BV421 (catalog 100335, clone 145-
658 2C11); CD3ε-FITC (catalog 553061, clone 145-2C11, BD Bioscience); CX3CR1-PE (catalog
659 149005, clone SA011F11); Ly6G-PerCP-Cy5.5 (catalog 127615, clone 1A8); Ly6C-BV510 (catalog
660 108437, clone RB6-8C5); F4/80-APC-Cy7 (catalog 123118, clone BM8). For mitochondrial
661 metabolic assay, fresh cells were incubated in 37℃ media for 30min with 100 nM MitoTracker
662 Green (catalog M7514, Invitrogen), 100 nM TMRM (catalog T668; Invitrogen), and 10 uM
663 MitoSOX Red (catalog M36008; Invitrogen), respectively. Surface-stained after washing with PBS
664 and then detected by flow cytometry. For intracellular IFN-γ staining, Cells freshly obtained from
665 liver and spleen were stimulated 12 hours with or without cytokine. GolgiStop (BD Biosciences)
666 was added 4 hours before intracellular staining.

667 **Bulk RNA sequencing**

668 Total RNA from FACS sorted splenic NK cells of *Prdm1*$^{+/+}$ and *Prdm1*$^{\Delta Ncr1}$ mice was extracted
669 by TRIzol reagent (Invitrogen), then reverse transcribed into cDNA. Library construction was
670 prepared using Illumina mRNA Library kit, and sequencing was performed by the BGISEQ-500.
671 Standard methods were used to analyze the RNA-seq data, including aligning the reads to the
672 genome by HISAT2 (v2.1.0) (72), and gene expression values (Counts) were calculated using
673 RSEM (v1.3.1) (73). DEGs were identified using DEseq2 (v1.4.5) (74) with a cutoff of $\log_2$(fold

674 change) > 0.5 and P < 0.05. The "clusterProfiler" package (v4.4.4) (75) and gene sets from molecular
675 signatures database (MSigDB) were used for GSEA and GO analysis. The heatmap was plotted
676 using the "Pheatmap" package (v1.0.12).

677 **Single-cell RNA sequencing**

678 FACS-sorted liver $CD45^{+}$ cells with more than 80% cell viability were used for library
679 preparation. Each sample contained cells from three *Prdm1*$^{+/+}$ or *Prdm1*$^{\Delta Ncr1}$ mice. Gel Bead-in-
680 Emulsions (GEMs) were generated using the 10X Genomics Chromium system, which combinates
681 Master Mix, Single Cell 3' v3.1 Gel Beads, and Partitioning Oil with single cells. GEMs were mixed
682 with cell lysate and reverse transcription reagent to produce full-length cDNA. After incubation, the
683 GEMs were broken, and recovered cDNA were amplified via PCR. Fragmentation, End repair, A-
684 tailing, and Adaptor Ligation were performed to obtain final libraries, which contain P5 and P7
685 sequences. The 3' library was sequenced on Novaseq 6000 with approximately 50k read pairs/cell
686 sequencing depth. The "Seurat" R package (v4.2.0) (76) was used for data analysis. Initial quality
687 control was performed to filter out the low-quality cells and cell doublets. Cells with 200-5500
688 expressed genes and no more than 10% mitochondrial genes were considered for high-quality.
689 Doublets were filtered with the "scDblFinder" Package (v1.10.0) (77). After quality control, we
690 totally recovered 6161 cells and 4817 cells from *Prdm1*$^{+/+}$ and *Prdm1*$^{\Delta Ncr1}$ mice, respectively.
691 Principal component analysis (PCA) was used for cluster analysis. The first 15 PCs were picked for
692 clustering and further visualized by UMAP. Clusters-specific marker was defined using the
693 "FindAllMarkers" function, and clusters were manually annotated based on the top 30 or 15 markers.
694 The "clusterProfiler" package and gene set from MSigDB were used for GSEA and GO analysis.

695 “CellChat” package (v1.4.0) (56) was utilized to predict the cell-to-cell communication from
696 scRNA-seq data.

697 **TCGA datasets assay**

698 The normalized gene expression and survival datasets of cancer patients collected in The
699 Cancer Genome Atlas (TCGA) were downloaded from UCSC Xena (http://xena.ucsc.edu/) (78).
700 NK cell-associated genes including *CD160*, *CD244*, *CTSW*, *FASLG*, *GZMA*, *GZMB*, *GZMH*,
701 *IL18RAP*, *IL2RB*, *KIR2DL4*, *KLRB1*, *KLRC3*, *KLRD1*, *KLRF1*, *KLRK1*, *NCR1*, *NKG7*, *PRF1*,
702 *XCL1*, *XCL2,* according to the previous study (33). NK cell-associated genes, together with *PRDM1*,
703 constitute the *NK-PRDM1* signature in this study. The mean expression of per genes was ordered
704 from high-to-low and plotted by heatmap using the “Pheatmap” package. The overall survival of
705 patients in the high and low expression of *NK-PRDM1* signature was selected for analysis. Kaplan-
706 Meier curves were plotted by GraphPad Prism.

707 **Statistics**

708 For experiment results, two-tailed t tests were used to measure the continuous and normally
709 distributed between the two independent groups. Paired t-tests were used to determine the statistical
710 significance between two paired groups. Log-rank tests were used to compare the overall survival
711 distribution between the two groups of patients. A P value less than 0.05 was considered significant
712 and data were presented as mean ± SEM.

713 **Study approval**

714 All animal experiments were approved by The Tianjin University Animal Care and Use

Committee. No human subjects were performed in this study.

Author contributions

Jitian He, and Youwei Wang designed experiments, performed experiments, analyzed the data and wrote the manuscript. Jitian He, Le Gao, Peiying Wang, Yiran Zheng, and Yumo Zhang performed experiments. Wing Keung Chan, Jiming Wang, Huaiyong Chen, and Zhouxin Yang analyzed the data, interpreted results and reviewed the manuscript.

Acknowledgments

This work was supported by National Key Research and Development Plan of China (2022YFF1202901); National Natural Science Foundation of China (82372801); and The Zhejiang Provincial Natural Science Foundation of China (LY21H150002).

Declaration of interests

The authors have declared that no conflict of interest exists.

References

1. Spits H, Artis D, Colonna M, Diefenbach A, Di Santo JP, Eberl G, et al. Innate lymphoid cells--a proposal for uniform nomenclature. *Nat Rev Immunol.* 2013;13(2):145-9.
2. Peng H, Jiang X, Chen Y, Sojka DK, Wei H, Gao X, et al. Liver-resident NK cells confer adaptive immunity in skin-contact inflammation. *J Clin Invest.* 2013;123(4):1444-56.
3. Bai L, Vienne M, Tang L, Kerdiles Y, Etiennot M, Escaliere B, et al. Liver type 1 innate lymphoid cells develop locally via an interferon-gamma-dependent loop. *Science.* 2021;371(6536).
4. Weizman OE, Adams NM, Schuster IS, Krishna C, Pritykin Y, Lau C, et al. ILC1 Confer Early Host Protection at Initial Sites of Viral Infection. *Cell.* 2017;171(4):795-808 e12.
5. Schuster IS, Wikstrom ME, Brizard G, Coudert JD, Estcourt MJ, Manzur M, et al. TRAIL+ NK cells control CD4+ T cell responses during chronic viral infection to limit autoimmunity. *Immunity.* 2014;41(4):646-56.
6. Ducimetiere L, Lucchiari G, Litscher G, Nater M, Heeb L, Nunez NG, et al. Conventional NK cells and tissue-resident ILC1s join forces to control liver metastasis. *Proc Natl Acad Sci U S A.* 2021;118(27).
7. Fumagalli V, Venzin V, Di Lucia P, Moalli F, Ficht X, Ambrosi G, et al. Group 1 ILCs regulate T cell-mediated liver immunopathology by controlling local IL-2 availability. *Science immunology.* 2022;7(68):eabi6112.
8. Kiessling R, Klein E, and Wigzell H. "Natural" killer cells in the mouse. I. Cytotoxic cells with specificity for mouse Moloney leukemia cells. Specificity and distribution according to genotype. *European journal of immunology.* 1975;5(2):112-7.
9. Nabekura T, Riggan L, Hildreth AD, O'Sullivan TE, and Shibuya A. Type 1 Innate Lymphoid Cells Protect Mice from Acute Liver Injury via Interferon-gamma Secretion for Upregulating Bcl-xL Expression in Hepatocytes. *Immunity.* 2020;52(1):96-108 e9.
10. Takeda K, Hayakawa Y, Smyth MJ, Kayagaki N, Yamaguchi N, Kakuta S, et al. Involvement of tumor necrosis factor-related apoptosis-inducing ligand in surveillance of tumor metastasis by liver natural killer cells. *Nat Med.* 2001;7(1):94-100.
11. Townsend MJ, Weinmann AS, Matsuda JL, Salomon R, Farnham PJ, Biron CA, et al. T-bet regulates the terminal maturation and homeostasis of NK and Valpha14i NKT cells. *Immunity.* 2004;20(4):477-94.
12. Yokota Y, Mansouri A, Mori S, Sugawara S, Adachi S, Nishikawa S, et al. Development of peripheral lymphoid organs and natural killer cells depends on the helix-loop-helix inhibitor Id2. *Nature.* 1999;397(6721):702-6.
13. Gascoyne DM, Long E, Veiga-Fernandes H, de Boer J, Williams O, Seddon B, et al. The basic leucine zipper transcription factor E4BP4 is essential for natural killer cell development. *Nature immunology.* 2009;10(10):1118-24.
14. Constantinides MG, McDonald BD, Verhoef PA, and Bendelac A. A committed precursor to innate lymphoid cells. *Nature.* 2014;508(7496):397-401.
15. Gordon SM, Chaix J, Rupp LJ, Wu J, Madera S, Sun JC, et al. The transcription factors T-bet and Eomes control key checkpoints of natural killer cell maturation. *Immunity.* 2012;36(1):55-67.

16. Daussy C, Faure F, Mayol K, Viel S, Gasteiger G, Charrier E, et al. T-bet and Eomes instruct the development of two distinct natural killer cell lineages in the liver and in the bone marrow. *J Exp Med.* 2014;211(3):563-77.
17. Mackay LK, Minnich M, Kragten NA, Liao Y, Nota B, Seillet C, et al. Hobit and Blimp1 instruct a universal transcriptional program of tissue residency in lymphocytes. *Science.* 2016;352(6284):459-63.
18. Lee JC, Green MD, Huppert LA, Chow C, Pierce RH, and Daud AI. The Liver-Immunity Nexus and Cancer Immunotherapy. *Clin Cancer Res.* 2022;28(1):5-12.
19. Galon J, and Bruni D. Approaches to treat immune hot, altered and cold tumours with combination immunotherapies. *Nature reviews Drug discovery.* 2019;18(3):197-218.
20. Ruff SM, Shannon AH, Beane JD, and Pawlik TM. Highlighting novel targets in immunotherapy for liver cancer. *Expert review of gastroenterology & hepatology.* 2022;16(11-12):1029-41.
21. He Y, Zhan L, Shi J, Xiao M, Zuo R, Wang C, et al. The Combination of R848 with Sorafenib Enhances Antitumor Effects by Reprogramming the Tumor Immune Microenvironment and Facilitating Vascular Normalization in Hepatocellular Carcinoma. *Adv Sci (Weinh).* 2023:e2207650.
22. Nersesian S, Schwartz SL, Grantham SR, MacLean LK, Lee SN, Pugh-Toole M, et al. NK cell infiltration is associated with improved overall survival in solid cancers: A systematic review and meta-analysis. *Transl Oncol.* 2021;14(1):100930.
23. Lee HA, Goh HG, Lee YS, Jung YK, Kim JH, Yim HJ, et al. Natural killer cell activity is a risk factor for the recurrence risk after curative treatment of hepatocellular carcinoma. *BMC Gastroenterol.* 2021;21(1):258.
24. Gao Y, Souza-Fonseca-Guimaraes F, Bald T, Ng SS, Young A, Ngiow SF, et al. Tumor immunoevasion by the conversion of effector NK cells into type 1 innate lymphoid cells. *Nature immunology.* 2017;18(9):1004-15.
25. Wang Y, Chu J, Yi P, Dong W, Saultz J, Wang Y, et al. SMAD4 promotes TGF-beta-independent NK cell homeostasis and maturation and antitumor immunity. *J Clin Invest.* 2018;128(11):5123-36.
26. Cortez VS, Ulland TK, Cervantes-Barragan L, Bando JK, Robinette ML, Wang Q, et al. SMAD4 impedes the conversion of NK cells into ILC1-like cells by curtailing non-canonical TGF-beta signaling. *Nat Immunol.* 2017;18(9):995-1003.
27. Keller AD, and Maniatis T. Identification and characterization of a novel repressor of beta-interferon gene expression. *Genes Dev.* 1991;5(5):868-79.
28. Kallies A, Hawkins ED, Belz GT, Metcalf D, Hommel M, Corcoran LM, et al. Transcriptional repressor Blimp-1 is essential for T cell homeostasis and self-tolerance. *Nat Immunol.* 2006;7(5):466-74.
29. Martins GA, Cimmino L, Shapiro-Shelef M, Szabolcs M, Herron A, Magnusdottir E, et al. Transcriptional repressor Blimp-1 regulates T cell homeostasis and function. *Nat Immunol.* 2006;7(5):457-65.
30. Kallies A, Carotta S, Huntington ND, Bernard NJ, Tarlinton DM, Smyth MJ, et al. A role for Blimp1 in the transcriptional network controlling natural killer cell maturation. *Blood.* 2011;117(6):1869-79.
31. Akman B, Hu X, Liu X, Hatipoglu T, You H, Chan WC, et al. PRDM1 decreases sensitivity of

817 human NK cells to IL2-induced cell expansion by directly repressing CD25 (IL2RA). *Journal*
818 *of leukocyte biology.* 2021;109(5):901-14.
819 32. Smith MA, Maurin M, Cho HI, Becknell B, Freud AG, Yu J, et al. PRDM1/Blimp-1 controls
820 effector cytokine production in human NK cells. *J Immunol.* 2010;185(10):6058-67.
821 33. Cursons J, Souza-Fonseca-Guimaraes F, Foroutan M, Anderson A, Hollande F, Hediyeh-Zadeh
822 S, et al. A Gene Signature Predicting Natural Killer Cell Infiltration and Improved Survival in
823 Melanoma Patients. *Cancer Immunol Res.* 2019;7(7):1162-74.
824 34. Shapiro-Shelef M, Lin K-I, McHeyzer-Williams LJ, Liao J, McHeyzer-Williams MG, and
825 Calame K. Blimp-1 Is Required for the Formation of Immunoglobulin Secreting Plasma Cells
826 and Pre-Plasma Memory B Cells. *Immunity.* 2003;19(4):607-20.
827 35. Hayakawa Y, and Smyth MJ. CD27 dissects mature NK cells into two subsets with distinct
828 responsiveness and migratory capacity. *J Immunol.* 2006;176(3):1517-24.
829 36. Chiossone L, Chaix J, Fuseri N, Roth C, Vivier E, and Walzer T. Maturation of mouse NK cells
830 is a 4-stage developmental program. *Blood.* 2009;113(22):5488-96.
831 37. Huntington ND, Tabarias H, Fairfax K, Brady J, Hayakawa Y, Degli-Esposti MA, et al. NK cell
832 maturation and peripheral homeostasis is associated with KLRG1 up-regulation. *J Immunol.*
833 2007;178(8):4764-70.
834 38. Bix M, Liao NS, Zijlstra M, Loring J, Jaenisch R, and Raulet D. Rejection of class I MHC-
835 deficient haemopoietic cells by irradiated MHC-matched mice. *Nature.* 1991;349(6307):329-
836 31.
837 39. Bern MD, Parikh BA, Yang L, Beckman DL, Poursine-Laurent J, and Yokoyama WM. Inducible
838 down-regulation of MHC class I results in natural killer cell tolerance. *The Journal of*
839 *experimental medicine.* 2019;216(1):99-116.
840 40. Karre K, Ljunggren HG, Piontek G, and Kiessling R. Selective rejection of H-2-deficient
841 lymphoma variants suggests alternative immune defence strategy. *Nature.* 1986;319(6055):675-
842 8.
843 41. Viant C, Fenis A, Chicanne G, Payrastre B, Ugolini S, and Vivier E. SHP-1-mediated inhibitory
844 signals promote responsiveness and anti-tumour functions of natural killer cells. *Nat Commun.*
845 2014;5:5108.
846 42. Cillo C, Dick JE, Ling V, and Hill RP. Generation of drug-resistant variants in metastatic B16
847 mouse melanoma cell lines. *Cancer Res.* 1987;47(10):2604-8.
848 43. Sathe P, Delconte RB, Souza-Fonseca-Guimaraes F, Seillet C, Chopin M, Vandenberg CJ, et al.
849 Innate immunodeficiency following genetic ablation of Mcl1 in natural killer cells. *Nat*
850 *Commun.* 2014;5:4539.
851 44. Robinette ML, Fuchs A, Cortez VS, Lee JS, Wang Y, Durum SK, et al. Transcriptional programs
852 define molecular characteristics of innate lymphoid cell classes and subsets. *Nat Immunol.*
853 2015;16(3):306-17.
854 45. Klose CS, Kiss EA, Schwierzeck V, Ebert K, Hoyler T, d'Hargues Y, et al. A T-bet gradient
855 controls the fate and function of CCR6-RORgammat+ innate lymphoid cells. *Nature.*
856 2013;494(7436):261-5.
857 46. Chen Y, Wang X, Hao X, Li B, Tao W, Zhu S, et al. Ly49E separates liver ILC1s into embryo-
858 derived and postnatal subsets with different functions. *The Journal of experimental medicine.*
859 2022;219(5).
860 47. Bottcher JP, Bonavita E, Chakravarty P, Blees H, Cabeza-Cabrerizo M, Sammicheli S, et al. NK

Cells Stimulate Recruitment of cDC1 into the Tumor Microenvironment Promoting Cancer Immune Control. *Cell.* 2018;172(5):1022-37 e14.

48. Kirchhammer N, Trefny MP, Natoli M, Brucher D, Smith SN, Werner F, et al. NK cells with tissue-resident traits shape response to immunotherapy by inducing adaptive antitumor immunity. *Sci Transl Med.* 2022;14(653):eabm9043.

49. Di Censo C, Marotel M, Mattiola I, Muller L, Scarno G, Pietropaolo G, et al. Granzyme A and CD160 expression delineates ILC1 with graded functions in the mouse liver. *European journal of immunology.* 2021;51(11):2568-75.

50. Friedrich C, Taggenbrock R, Doucet-Ladeveze R, Golda G, Moenius R, Arampatzi P, et al. Effector differentiation downstream of lineage commitment in ILC1s is driven by Hobit across tissues. *Nat Immunol.* 2021;22(10):1256-67.

51. Flommersfeld S, Bottcher JP, Ersching J, Flossdorf M, Meiser P, Pachmayr LO, et al. Fate mapping of single NK cells identifies a type 1 innate lymphoid-like lineage that bridges innate and adaptive recognition of viral infection. *Immunity.* 2021;54(10):2288-304 e7.

52. Yomogida K, Bigley TM, Trsan T, Gilfillan S, Cella M, Yokoyama WM, et al. Hobit confers tissue-dependent programs to type 1 innate lymphoid cells. *Proc Natl Acad Sci U S A.* 2021;118(50).

53. Tu Z, Bozorgzadeh A, Pierce RH, Kurtis J, Crispe IN, and Orloff MS. TLR-dependent cross talk between human Kupffer cells and NK cells. *J Exp Med.* 2008;205(1):233-44.

54. Park MD, Reyes-Torres I, LeBerichel J, Hamon P, LaMarche NM, Hegde S, et al. TREM2 macrophages drive NK cell paucity and dysfunction in lung cancer. *Nat Immunol.* 2023;24(5):792-801.

55. Heymann F, Peusquens J, Ludwig-Portugall I, Kohlhepp M, Ergen C, Niemietz P, et al. Liver inflammation abrogates immunological tolerance induced by Kupffer cells. *Hepatology.* 2015;62(1):279-91.

56. Jin S, Guerrero-Juarez CF, Zhang L, Chang I, Ramos R, Kuan CH, et al. Inference and analysis of cell-cell communication using CellChat. *Nat Commun.* 2021;12(1):1088.

57. Takeda K, Nakayama M, Sakaki M, Hayakawa Y, Imawari M, Ogasawara K, et al. IFN-gamma production by lung NK cells is critical for the natural resistance to pulmonary metastasis of B16 melanoma in mice. *Journal of leukocyte biology.* 2011;90(4):777-85.

58. Lin Q, Rong L, Jia X, Li R, Yu B, Hu J, et al. IFN-gamma-dependent NK cell activation is essential to metastasis suppression by engineered Salmonella. *Nature communications.* 2021;12(1):2537.

59. Roe K. NK-cell exhaustion, B-cell exhaustion and T-cell exhaustion-the differences and similarities. *Immunology.* 2022;166(2):155-68.

60. Zhang Q, Bi J, Zheng X, Chen Y, Wang H, Wu W, et al. Blockade of the checkpoint receptor TIGIT prevents NK cell exhaustion and elicits potent anti-tumor immunity. *Nature Immunology.* 2018;19(7):723-32.

61. Sciume G, De Angelis G, Benigni G, Ponzetta A, Morrone S, Santoni A, et al. CX3CR1 expression defines 2 KLRG1+ mouse NK-cell subsets with distinct functional properties and positioning in the bone marrow. *Blood.* 2011;117(17):4467-75.

62. Chea S, Possot C, Perchet T, Petit M, Cumano A, and Golub R. CXCR6 Expression Is Important for Retention and Circulation of ILC Precursors. *Mediators Inflamm.* 2015;2015:368427.

63. Hudspeth K, Donadon M, Cimino M, Pontarini E, Tentorio P, Preti M, et al. Human liver-

905 resident CD56(bright)/CD16(neg) NK cells are retained within hepatic sinusoids via the
906 engagement of CCR5 and CXCR6 pathways. *Journal of autoimmunity.* 2016;66:40-50.
907 64. Lynn RC, Weber EW, Sotillo E, Gennert D, Xu P, Good Z, et al. c-Jun overexpression in CAR
908 T cells induces exhaustion resistance. *Nature.* 2019;576(7786):293-300.
909 65. Wu H, Zhao X, Hochrein SM, Eckstein M, Gubert GF, Knopper K, et al. Mitochondrial
910 dysfunction promotes the transition of precursor to terminally exhausted T cells through HIF-
911 1alpha-mediated glycolytic reprogramming. *Nature communications.* 2023;14(1):6858.
912 66. Zheng X, Qian Y, Fu B, Jiao D, Jiang Y, Chen P, et al. Mitochondrial fragmentation limits NK
913 cell-based tumor immunosurveillance. *Nature immunology.* 2019;20(12):1656-67.
914 67. Cheng HP, Huang CJ, Tsai ML, Ong HT, Cheong SK, Choo KB, et al. MicroRNA-362
915 negatively and positively regulates SMAD4 expression in TGF-beta/SMAD signaling to
916 suppress cell migration and invasion. *Int J Med Sci.* 2021;18(8):1798-809.
917 68. Jeevan-Raj B, Gehrig J, Charmoy M, Chennupati V, Grandclement C, Angelino P, et al. The
918 Transcription Factor Tcf1 Contributes to Normal NK Cell Development and Function by
919 Limiting the Expression of Granzymes. *Cell reports.* 2017;20(3):613-26.
920 69. Guo H, Wang M, Wang B, Guo L, Cheng Y, Wang Z, et al. PRDM1 Drives Human Primary T
921 Cell Hyporesponsiveness by Altering the T Cell Transcriptome and Epigenome. *Front Immunol.*
922 2022;13:879501.
923 70. Babichuk CK, and Bleackley RC. Mutational analysis of the murine granzyme B gene promoter
924 in primary T cells and a T cell clone. *J Biol Chem.* 1997;272(30):18564-71.
925 71. Kucuk C, Iqbal J, Hu X, Gaulard P, De Leval L, Srivastava G, et al. PRDM1 is a tumor
926 suppressor gene in natural killer cell malignancies. *Proc Natl Acad Sci U S A.*
927 2011;108(50):20119-24.
928 72. Kim D, Langmead B, and Salzberg SL. HISAT: a fast spliced aligner with low memory
929 requirements. *Nat Methods.* 2015;12(4):357-60.
930 73. Li B, and Dewey CN. RSEM: accurate transcript quantification from RNA-Seq data with or
931 without a reference genome. *BMC Bioinformatics.* 2011;12:323.
932 74. Love MI, Huber W, and Anders S. Moderated estimation of fold change and dispersion for
933 RNA-seq data with DESeq2. *Genome Biol.* 2014;15(12):550.
934 75. Wu T, Hu E, Xu S, Chen M, Guo P, Dai Z, et al. clusterProfiler 4.0: A universal enrichment tool
935 for interpreting omics data. *Innovation (Camb).* 2021;2(3):100141.
936 76. Hao Y, Hao S, Andersen-Nissen E, Mauck WM, 3rd, Zheng S, Butler A, et al. Integrated analysis
937 of multimodal single-cell data. *Cell.* 2021;184(13):3573-87 e29.
938 77. Germain PL, Lun A, Garcia Meixide C, Macnair W, and Robinson MD. Doublet identification
939 in single-cell sequencing data using scDblFinder. *F1000Res.* 2021;10:979.
940 78. Caicedo HH, Hashimoto DA, Caicedo JC, Pentland A, and Pisano GP. Overcoming barriers to
941 early disease intervention. *Nat Biotechnol.* 2020;38(6):669-73.

942

Graphical abstract

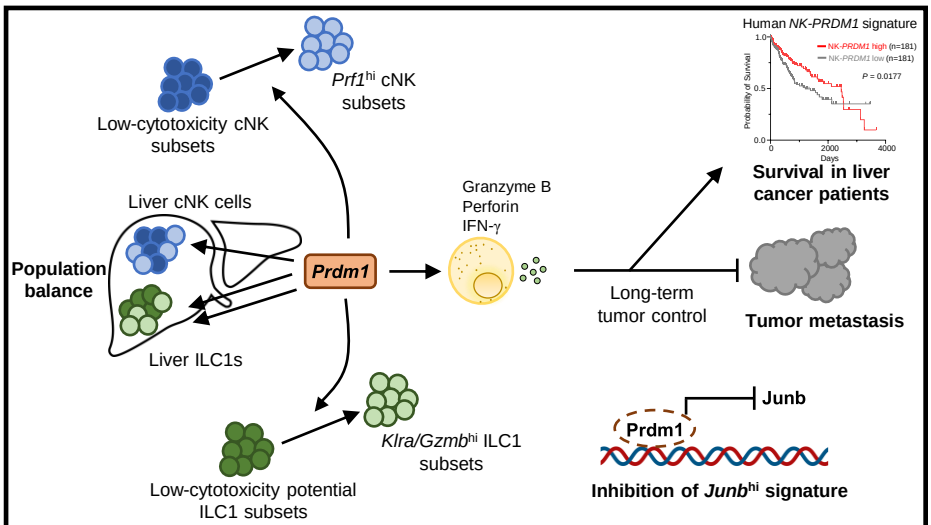

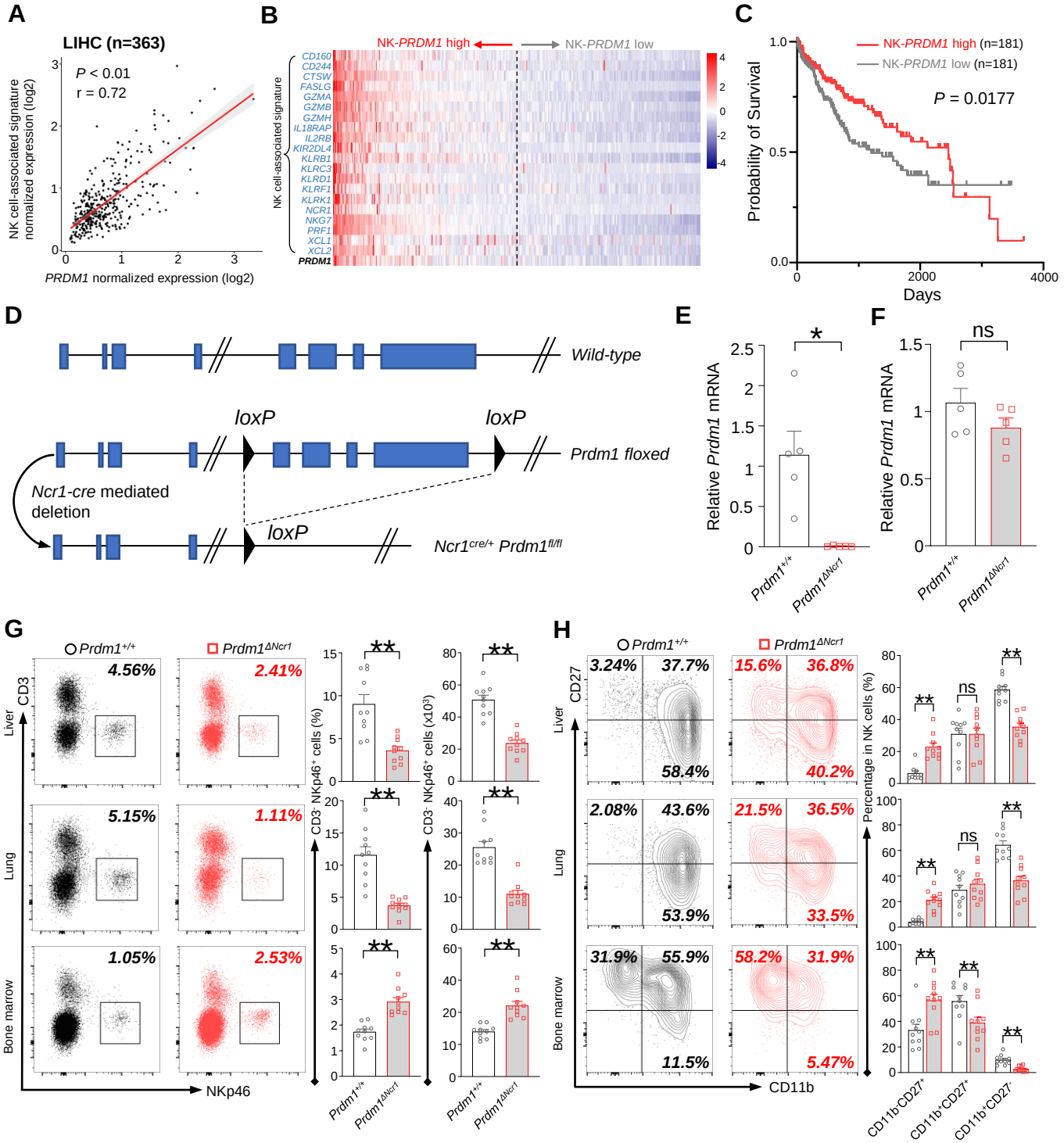

Figure 1. *Prdm1* promotes NK cell homeostasis and terminal maturation.
(**A**) Correlation between the average expression of NK cell-associated signature and *PRDM1* in LIHC (Liver Hepatocellular Carcinoma; n=363) patients sourced from TCGA datasets. (**B**) Heatmap of the ordered, z-score normalized expression values for *PRDM1* and NK cell-associated genes in liver cancer patients. High and low expression of *NK-PRDM1* signature are indicated. (**C**) Prognostic value of the *NK-PRDM1* signature for overall survival of liver cancer patients comparing high and low samples with a median cutoff. (**D**) Schematic representation of the Prdm1-conditional knockout mouse model. Targeted exon 6-8 of *Prdm1* (top) is flanked with *loxP* sites (middle). Ncr1-expressed Cre recombinase was used to generate the *Prdm1*$^{\Delta Ncr1}$ allele (bottom). (**E** and **F**) Real-time RT-PCR quantification of *Prdm1* expression in NKp46^{+} cells (**E**) and splenocytes (**F**) to determine the presence of *Prdm1* (n=5). (**G**) Representative flow cytometric plots (left) and quantification (right) of the proportion and absolute number of CD45^{+}CD3^{-}NKp46^{+} cells among lymphocytes in liver, lung, and bone marrow (n=10). (**H**) Representative flow cytometric plots (left) of the CD11b and CD27 expression within CD3^{-}NK1.1^{+}NKp46^{+}CD49b^{+} cells in liver, lung, and bone marrow (n=10). Right panel showed the percentage of distinct maturation stages of NK cells. Data are presented as the mean±SEM and were analyzed by 2-tailed, paired t-test. Differences were evaluated between littermates. Each circle and square on graphs represents an individual mouse; *P*, *P*-value; r, pearson correlation coefficient; *, *P*<0.05; **, *P*<0.01, ns, not significant.

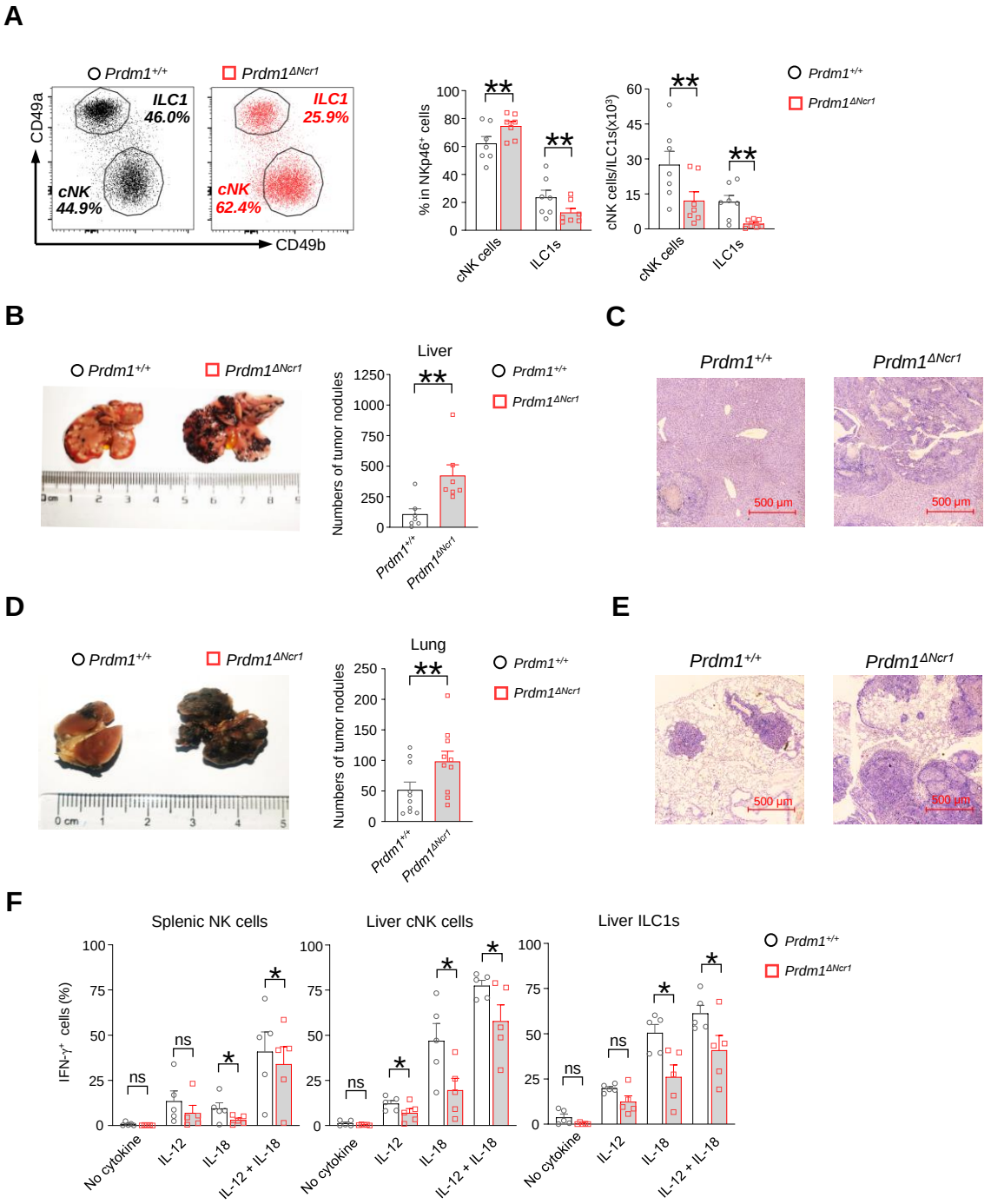

Figure 2. *Prdm1* is required for group 1 ILCs to control tumor metastasis.
(**A**) Representative flow cytometric plots (left) of liver cNK cells (CD49a$^-$CD49b$^+$) and ILC1s (CD49a$^+$CD49b$^-$) from *Prdm1*$^{+/+}$ and *Prdm1*$^{\Delta Ncr1}$ mice. The two bar graphs (right) quantitate the percentages and absolute numbers of cells respectively (n=7). (**B** and **D**) Representative image (left) and quantification (right) of tumor nodes on the livers (n=7) (**B**) and lungs (n=10) (**D**) of *Prdm1*$^{+/+}$ and *Prdm1*$^{\Delta Ncr1}$ mice at day 14 or 21 after inoculation with B16F10 melanoma cells. (**C** and **E**) Representative histopathological images of liver (**C**) and lung (**E**) tissues stained by hematoxylin-eosin to detect tumor metastasis. Red bar indicates 500 μm distance under the microscope. (**F**) Liver cells and splenocytes were co-stimulated in the presence or absence of IL-12 and IL-18 for 12 hours. GolgiStop was added 4 hours before intracellular staining of IFN-γ. The graphs showed percentage of IFN-γ$^+$ splenic cNK cells, liver cNK cells and ILC1s from *Prdm1*$^{+/+}$ and *Prdm1*$^{\Delta Ncr1}$ mice (n=5). Data are presented as the mean±SEM and were analyzed by 2-tailed, paired t-test. Differences were evaluated between littermates. Each circle and square on graphs represents an individual mouse; *P*, *P*-value; *, *P*<0.05; **, *P*<0.01, ns, not significant.

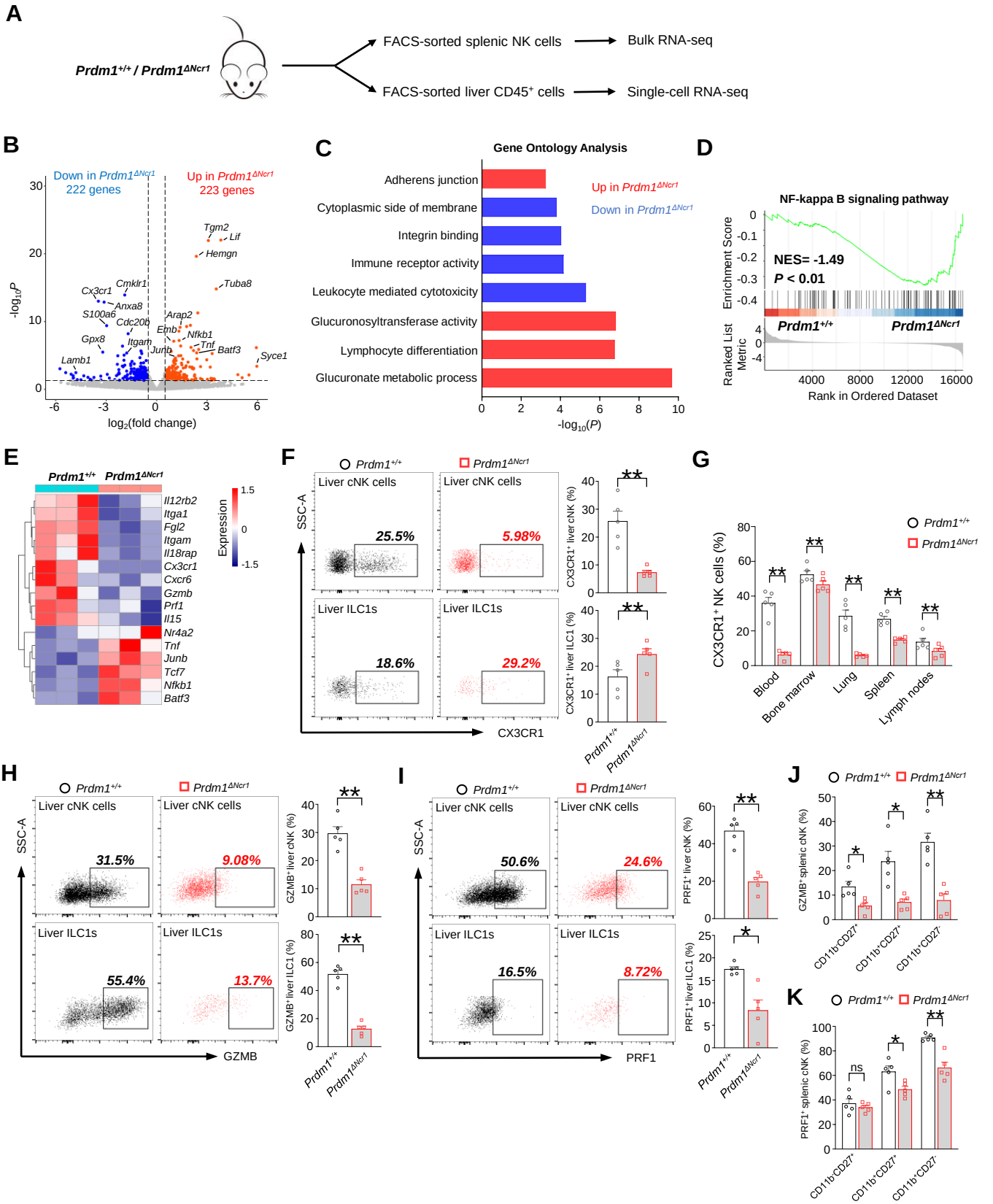

Figure 3. Bulk RNA-seq reveals *Prdm1*-mediated functions in splenic cNK cells.
(**A**) Splenic cNK cells and liver CD45$^+$ cells were sorted from *Prdm1*$^{+/+}$ and *Prdm1*$^{\Delta Ncr1}$ mice using flow cytometry, and prepared for bulk RNA-seq and single-cell RNA-seq analysis. (**B**) Volcano plot of the bulk RNA-seq differentially expressed genes (DEGs) ($\log_2$|fold change|>0.5; P<0.05) in splenic cNK cells between *Prdm1*$^{+/+}$ and *Prdm1*$^{\Delta Ncr1}$ mice. Upregulated and downregulated genes in *Prdm1*$^{\Delta Ncr1}$ cells were highlighted in red and blue. (**C**) Enriched Gene Ontology (GO) terms of DEGs in *Prdm1*$^{\Delta Ncr1}$ cells compared *Prdm1*$^{+/+}$ cells. The Enrichment gene set in upregulated (red) and downregulated (blue) genes were indicated in different colour. Bar length represents statistical significance. (**D**) Gene Set Enrichment Analysis (GSEA) showing the enrichment of NF-kappa B signaling pathway of DEGs in *Prdm1*$^{\Delta Ncr1}$ cells compared *Prdm1*$^{+/+}$ cells. NES, normalized enrichment score. (**E**) Heatmap of selected genes from DEGs. Shown is z-score transformed expression of DEGs. (**F**) Representative flow cytometric plots (left) and cumulative data (right) of the percentage and absolute numbers of CX3CR1$^+$ cells in liver cNK cells and ILC1s (n=5). (**G**) Quantification of CX3CR1$^+$ cells in NK cells in blood, bone marrow, lung, liver, spleen, and lymph nodes (n=5). (**H** and **I**) Representative flow cytometric plots (left) and cumulative data (right) showing the proportion of GZMB$^+$ (**H**) and PRF1$^+$ (**J**) liver cNK cells and ILC1s from *Prdm1*$^{+/+}$ and *Prdm1*$^{\Delta Ncr1}$ mice (n=5). (**J** and **K**) Proportion of GZMB$^+$ (**J**) and PRF1$^+$ (**K**) splenic NK cells at different maturation stages was analyzed by flow cytometry (n=5). Data are presented as the mean±SEM and were analyzed by 2-tailed, paired t-test. Differences were evaluated between littermates. Each circle and square on graphs represents an individual mouse; P, P-value; *, P<0.05; **, P<0.01, ns, not significant.

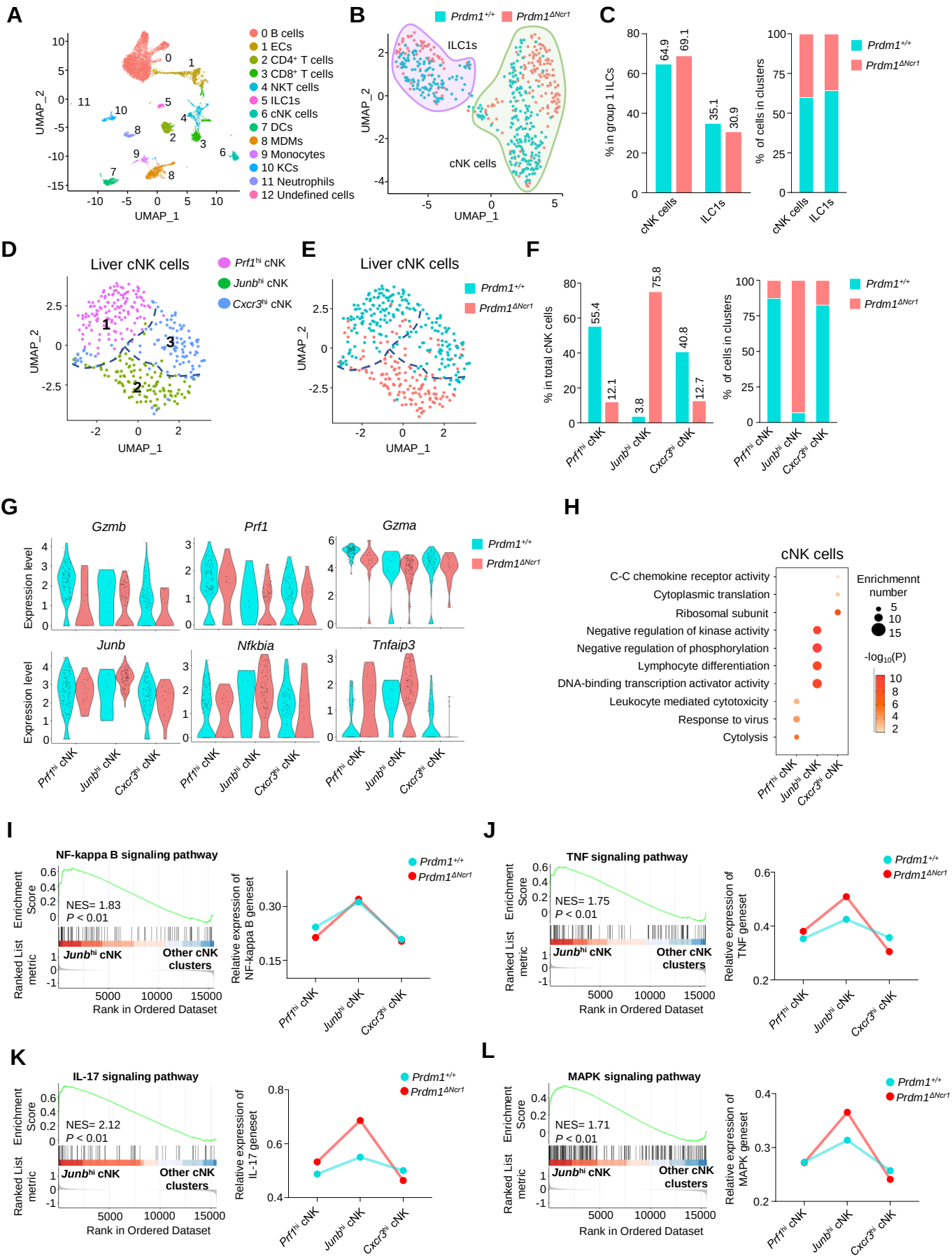

Figure 4. Different properties of cNK clusters following *Prdm1* knockout.
(**A**) Uniform manifold approximation and projection (UMAP) visualization of liver CD45$^+$ cells from *Prdm1*$^{+/+}$ and *Prdm1*$^{\Delta Ncr1}$ mice. Twelve clusters were defined and indicated by distinct colours. Each dot represents a single cell. (**B**) UMAP visualization of liver cNK and ILC1 clusters. Cells were colored by genotypes (*Prdm1*$^{+/+}$-blue; *Prdm1*$^{\Delta Ncr1}$-red). (**C**) Percentages of cNK cells and ILC1s in total group 1 ILCs (left), and their distribution in each cluster (right). (**D** and **E**) UMAP visualization of three different liver cNK clusters from two mouse strains. (**F**) Proportions of cNK cells among total cNK cells (left; 211 cells in *Prdm1*$^{+/+}$, and 141 cells in *Prdm1*$^{\Delta Ncr1}$) and within clusters (right). (**G**) Violin plots showing the normalized expression of select genes in different cNK clusters. (**H**) Enriched GO term of marker genes in three cNK clusters. Dot size represents enriched gene number, and color intensity represents significance. (**I-L**) GSEA plots (left) depicting the enrichment of NF-kappa B (**I**) , TNF (**J**) , IL-17 (**K**) , and MAPK (**L**) signaling pathway in *Junb*^{hi} cNK cluster compared with clusters of *Prf1*^{hi} and *Cxcr3*^{hi} cNK cells. Right panel showed dynamic relative expression of the given gene sets from cluster1 to cluster3 between *Prdm1*$^{+/+}$ and *Prdm1*$^{\Delta Ncr1}$. Dots represent the average expression of given gene set in each cell, which was calculated through the sum of normalized expression of each individual gene within the designated gene set in every single cell. NES, normalized enrichment score.

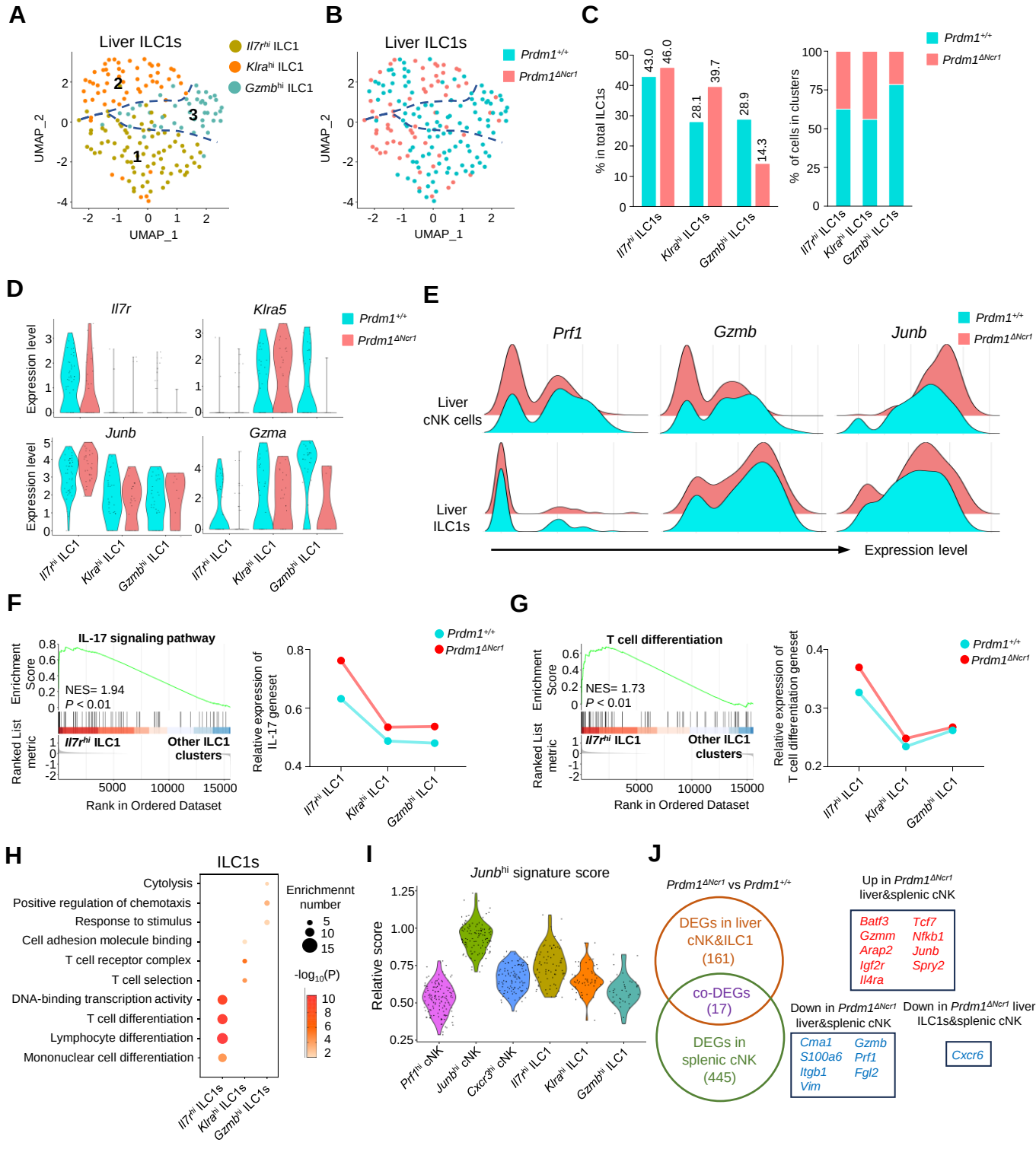

Figure 5. Different properties of ILC1 clusters following *Prdm1* knockout..
(**A and B**) UMAP visualization of three different liver ILC1 clusters from two mouse strains. (**C**) Proportions of ILC1s among total ILC1s in different genotypes (left; 114 cells in *Prdm1*$^{+/+}$, and 63 cells in *Prdm1*$^{\Delta Ncr1}$) and within each cluster (right). (**D**) Violin plots showing the normalized expression of select genes in different ILC1 clusters. (**E**) Ridge plots showing the normalized expression of *Gzmb, Prf1*, and *Junb* in cNK and ILC1 clusters between *Prdm1*$^{+/+}$ and *Prdm1*$^{\Delta Ncr1}$ cells. (**F** and **G**) GSEA plots (left) depicting the enrichment of IL-17 signaling pathway (**F**) and T cell differentiation (**G**) in *Il7r*^{hi} ILC1 cluster compared with clusters of *Klra*^{hi} and *Gzmb*^{hi} ILC1s. Right panel showed dynamic relative expression of the given gene sets from cluster1 to cluster3 between *Prdm1*$^{+/+}$ and *Prdm1*$^{\Delta Ncr1}$. Dots represent the average expression of given gene set in each cell, which was calculated through the sum of normalized expression of each individual gene within the designated gene set in every single cell. NES, normalized enrichment score. (**H**) Enriched GO term of marker genes in three ILC1 clusters. Dot size represents enriched gene number, and color intensity represents significance. (**I**) Violin plot showing the *Junb*^{hi} signature score for cNK cell and ILC1 clusters, calculated using the signature genes of *Junb*^{hi} cNK cluster. (**J**) Venn diagram showing overlapping and unique DEGs in comparisons within liver cNK cells, ILC1s and splenic cNK cells between *Prdm1*$^{+/+}$ and *Prdm1*$^{\Delta Ncr1}$(left), and 17 overlapped DEGs were shown at the right panel.

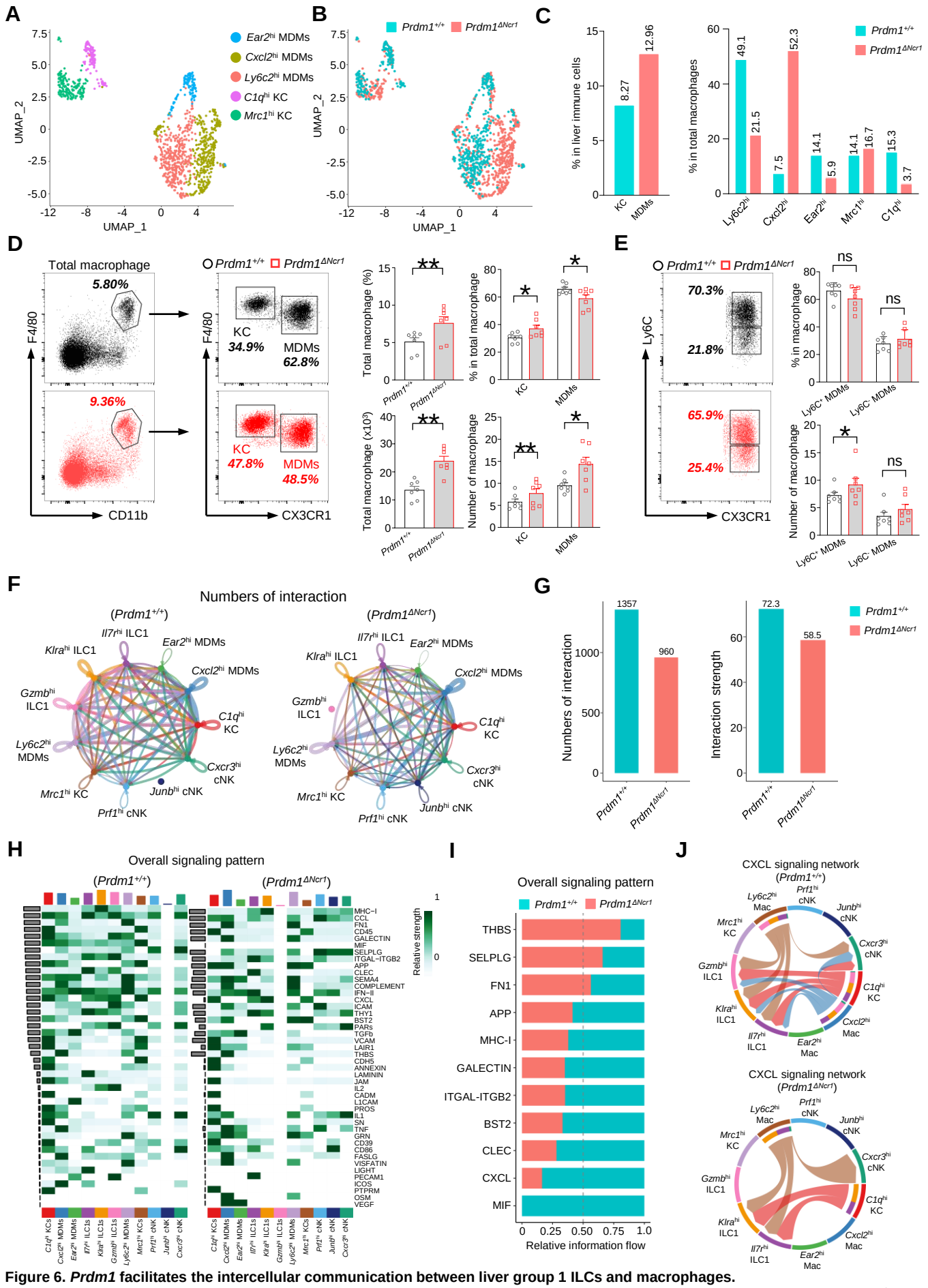

Figure 6. *Prdm1* facilitates the intercellular communication between liver group 1 ILCs and macrophages.
(**A** and **B**) UMAP visualization of monocyte-derived macrophages (MDMs) and Kupffer cells (KCs) cluster (**A**) between *Prdm1*$^{+/+}$ and *Prdm1*$^{\Delta Ncr1}$ (**B**). (**C**) Proportions of total macrophages in liver immune cells (left), and proportions of MDMs and KCs among total macrophages in different genotypes (510 cells in *Prdm1*$^{+/+}$, and 624 cells in *Prdm1*$^{\Delta Ncr1}$). (**D**) Representative flow cytometric plots (left) and cumulative data (right) of the percentage and absolute numbers of liver total macrophages (CD45^{+}Ly6G^{-}CD11b^{+}F4/80^{+}), MDMs (CX3CR1^{-}), and KCs (CX3CR1^{+}) between *Prdm1*$^{+/+}$ and *Prdm1*$^{\Delta Ncr1}$ (n=7). (**E**) Representative flow cytometric plots (left) and cumulative data (right) of the percentage and absolute numbers of Ly6C^{-} and Ly6C^{+} cells in MDMs. (**F** and **G**) Circle plots (**F**) and summary data (**G**) illustrating the interaction numbers and strength of significant enriched ligand–receptor pairs among cluster of liver cNK cells, ILC1s, and macrophages from *Prdm1*$^{+/+}$ (left) and *Prdm1*$^{\Delta Ncr1}$ (right) cells. The thickness of the line indicates the number of enrich pairs, and the arrow reflects the direction of the interaction. (**H**) Heatmap of overall signaling pattern recognized from ligand-receptor pairs, which contained the sum of signaling from the sender and target cells. (**I**) Bar graphs showing the information flow in selected active signaling patterns between *Prdm1*$^{+/+}$ and *Prdm1*$^{\Delta Ncr1}$ cells. Relative information flow was calculated as the sum of the communication probability in given signaling patterns. (**J**) Chord plot of the CXCL signaling interaction network among cluster of liver cNK cells, ILC1s, and macrophages between *Prdm1*$^{+/+}$ and *Prdm1*$^{\Delta Ncr1}$ cells. Data are presented as the mean±SEM and were analyzed by 2-tailed, paired t-test. Differences were evaluated between littermates. Each circle and square on graphs represents an individual mouse; *P*, *P*-value; *, *P*<0.05; **, *P*<0.01, ns, not significant.

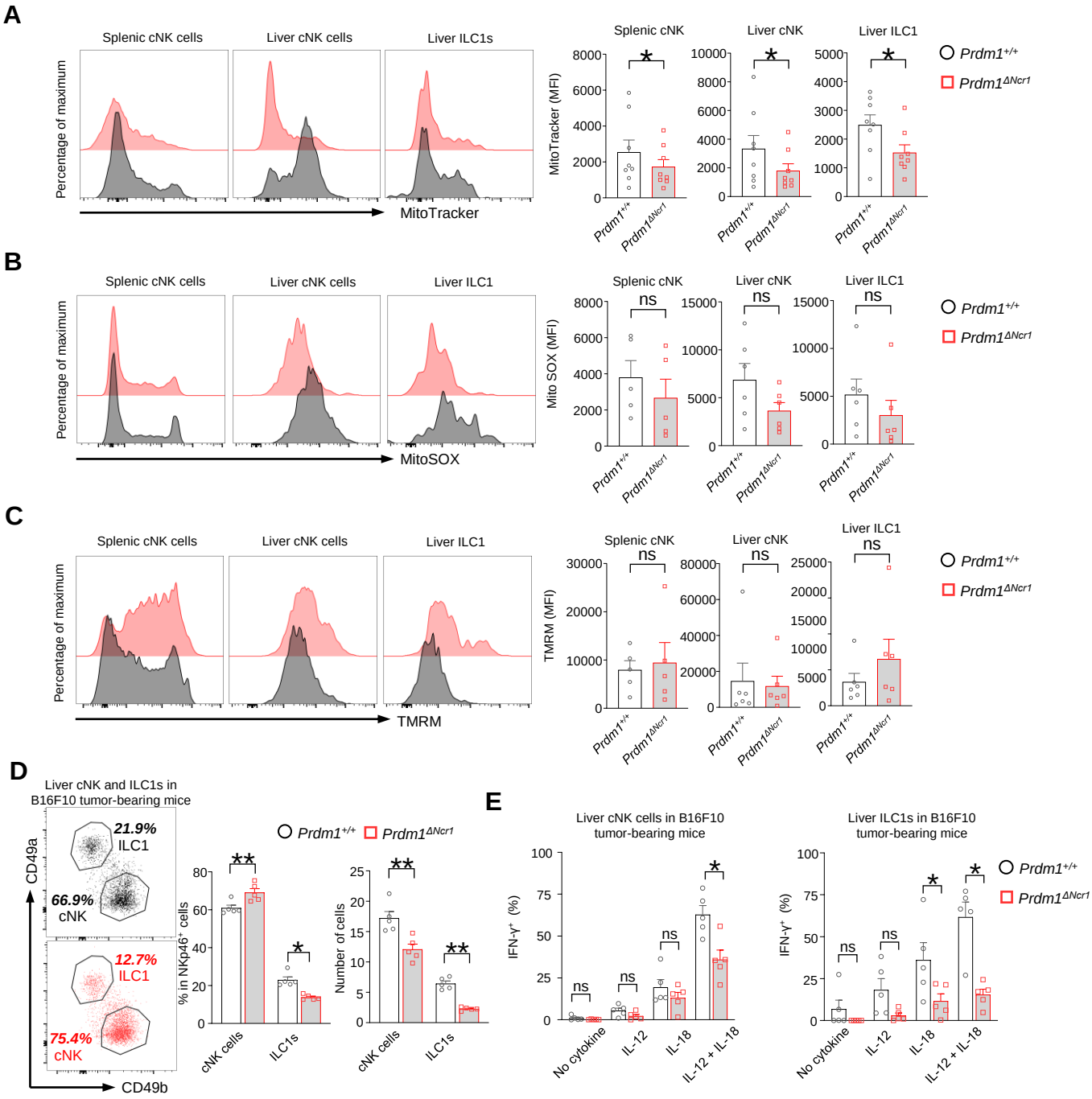

Figure 7. *Prdm1* safeguards group 1 ILCs from exhaustion-like phenotypes in the tumor microenvironment.
(A-C) The Mitochondrial mass (MitoTracker Green staining; n=8) (**A**), Mitochondrial ROS (MitoSOX staining; n=5) (**B**), and Mitochondrial membrane potential (TMRM staining; n=5) (**C**) of splenic cNK cells, liver cNK cells and ILC1s were analyzed by flow cytometry. Representative flow cytometric plots (left) and cumulative data (right) showing the relative mean fluorescence intensities (MFIs) of each group. (**D**) Representative flow cytometric plots (left) and cumulative data (right) showing the percentage and absolute number of liver cNK cells and ILC1s in *Prdm1*$^{+/+}$ and *Prdm1*$^{\Delta Ncr1}$ tumor-bearing mice at day 14 after inoculation with B16F10 melanoma cells via intrasplenic injection(n=5). (**E**) Percentages of IFN-γ^{+} liver cNK cells and ILC1s from *Prdm1*$^{+/+}$ and *Prdm1*$^{\Delta Ncr1}$ tumor-bearing mice (n=5). Data are presented as the mean±SEM and were analyzed by 2-tailed, paired t-test. Differences were evaluated between littermates. Each circle and square on graphs represents an individual mouse; *P*, *P*-value; *, *P*<0.05; **, *P*<0.01, ns, not significant.